C.1

Interaction Notes

Note 431

July 1982

SINGULARITY EXPANSION OF ELECTROMAGNETIC SCATTERING FROM THIN AND THICK CLOSED CYLINDERS

John L. Roberts
L. Wilson Pearson
Electrical Engineering Department
University of Mississippi
University, Mississippi 38677

ABSTRACT

The results of a numerical study undertaken to determine the singularity expansion paprameters of a closed, thin-walled cylinder are presented and discussed. The behavior of the SEM parameters is explained in terms of manifesting physical phenomena. The expansion parameters of the closed cylinder are compared to those of approximating structures, namely, the open cylinder and prolate spheroid. The propensity to radiate is observed to decrease when the caps and cylinder wall resonate more-or-less independently. Radiation due to torsional charge flow paths causes greater damping of the natural modes in the case of nonconstant azimuthal variation as opposed to that of constant variation; furthermore, the torsional radiation mechanism appears to dominate over endcap effects. Support is provided for the conjecture due to Wilton that the infinite families of nearly periodic poles lying near the frequency axis of the thin-wire loop are related to the interior resonances for closed strucutres. These families for the open cylinder are observed to track toward purely imaginary cavity resonances as the tube ends are closed. Selected SEM data are presented in support of these and other conclusions.

TABLE OF CONTENTS

LIST OF FIGURES

CHAPTER 1

INTRODUCTION

This work considers the Singularity Expansion Method (SEM) characterization of electromagnetic scattering by a thin-walled, closed cylinder. The cylinder, itself, can be very thin, such as treated by conventional "thin-wire" theory, or fairly thick with a length/diameter ratio approaching unity. The data obtained through the work reported here will ultimately be used to estimate complex resonances of the induced surface current on the object for time-harmonic excitations.

Work in the resonant behavior of cylindrical structures was first reported by Abraham [1] in the late nineteenth century. He used a prolate spheroid to model a cylinder, and computed the resonances of a spheroid with eccentricity one. Page and Adams [2], in 1938, and in work continuing in 1944 [3-4], modeled a thin cylinder as a prolate spheroid, with eccentricities ranging from unity to infinity. Their analytic investigation yielded resonant frequencies and currents.

The Singularity Expansion Method (SEM) was introduced by Baum in 1971, [5]. SEM was originally postulated for the prediction of transient scattering responses, however, it has equal utility in frequency-domain applications. Following Baum's postulation of SEM, Tesche [6] used the Singularity Expansion Method representation for current on a thin wire to determine the the frequency-dependent admittance of a center-driven, wire antenna.

Subsequently, Marin [7], in a numerical investigation, calculated the resonant frequencies and induced charges on a prolate spheroid to obtain the time response of the current and induced charge on a prolate spheroid. More recently, Melson and Pearson [8] have obtained, through a numerical exercise, the SEM representation of both thin and thick open cylinders.

Because it is the prototypical shape for a wide variety of missile structures, the thick, capped cylinder is an important object to study. The shape of appropriate cylinder models range from moderately thin, to moderately thick—sufficiently that the azimuthal variation of currents becomes significant. Once the azimuthal variation becomes significant, thin wire models become unacceptable, and models such as the one reported here become desirable. A missile can be modeled as a coaxial cylinder pair, where the cylinders have nearly equal radii. A cylinder with a suitably large diameter hole on either end, is a satisfactory model for such a structure. Since a scatterer can be thought of as a distributed network, it is possible to describe the scattering process by an equivalent circuit using synthesis techniques to synthesize (perhaps approximately) the appropriate complex transfer function of the scatterer. This work is a first step toward that synthesis, in that the synthesis requires the SEM descriptors.

The computational model used in this work takes account of azimuthal variation via, the more general, body of revolution approach of Mautz and Harrington [9], and of Glisson and Wilton [10]. As in the body of revolution solution of Glisson and Wilton, an electric field integral equation modeled the structure, and a Method

of Moments expansion that was employed to solve it, as well as a discussion of the numerical procedure's validations. The third chapter contains selected results and their physical interpretations. In Chapter 4, conclusions are drawn from the study.

CHAPTER 2

DESCRIPTION OF FORMULATION

2.1 Introduction

An electric field, integral equation was used to characterize scattering by a perfectly conducting, closed cylinder. The Method of Moments procedure, employing subsectional bases and collocation testing, was used to solve the integral equation. The Body of Revolution technique of Glisson and Wilton [10] was implemented to reduce the two dimensional character of the problem to a single dimensional one. Symmetry was exploited to further decrease the number of unknowns, and to permit the determination of both the so-called "even" and "odd" poles. This chapter reports details of the applied numerical formulation. This formulation follows previous work by others [10] in most respects and no claim to originality is made in connection with the present work. It is provided here for the sake of completeness.

2.2 Formulation of the Integral Equations

The ensuing material follows directly from the Body of Revolution approach of Glisson and Wilton [10], where their, arbitrary body is particularized to a perfectly conducting, closed cylinder. Consider the cylinder shown in Figure 1. The body is formed by rotating a planar arc, the generating curve, about the z-axis of the body of revolution. The t-coordinate, depicted in Figure 1, follows the generating curve on the body surface, S.

The perfectly conducting body is immersed in an infinite-extent, homogeneous medium, having constitutive parameters (μ,ε).

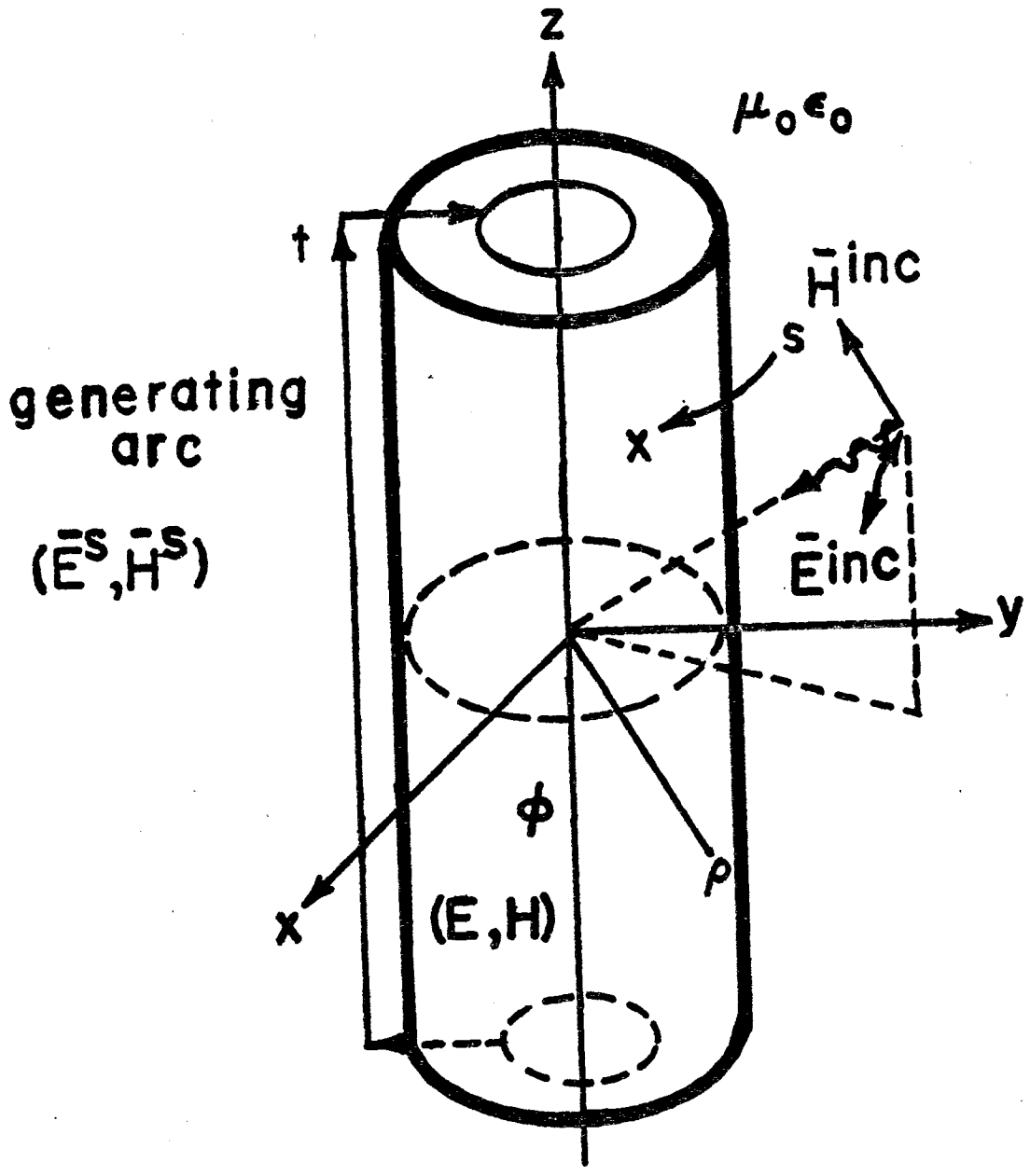

Figure 1. Geometry of the cylinder.

Since the cylinder is assumed perfectly conducting, boundary conditions require that the total electric field tangential to the body surface vanish, hence:

$$-(n \times \bar{E}^{scat}(r)) = \hat{n} \times \bar{E}^{inc}(r), \quad \bar{r} \in S \tag{2.1}$$

where $\bar{E}^{scat}$ is the scattered electric field, $\bar{E}^{inc}$ is the incident electric field, $\bar{E}^{inc} + \bar{E}^{scat} = \bar{E}$, the total electric field present, and $\hat{n} = \hat{\phi} \times \hat{t}$ is the outward normal to the body surface. Via the equivalence principle, the material body is replaced by a current $\bar{J}$ in free space, flowing along the cylinder's original surface. This equivalent current is the sum of currents flowing on the interior and exterior walls of the cylinder shell in the original problem. Now, the scattered electric field may be expressed as

$$\bar{E}^{s}(\bar{r}) = -s\bar{A}(\bar{r}) - \nabla\Phi(\bar{r}) \quad [1] \tag{2.2}$$

where the potentials are defined as:

$$\bar{A}(\bar{r}) = \frac{\mu}{4\pi} \iint_{s} \bar{J}(\bar{r}')\, G(\bar{r},\bar{r}')dS' \tag{2.3a}$$

$$\bar{\Phi}(\bar{r}) = \frac{1}{4\pi\varepsilon} \iint_{s} \rho_s(\bar{r})\, G(\bar{r},\bar{r}')dS' \tag{2.3b}$$

and where

$$G(\bar{r},\bar{r}') = \exp(-sR/c)/R \tag{2.4a}$$

---

[1] The formulation of eqs. (2.2) through (2.5), where the variable $s = \sigma + j\omega$ has been introduced, follows directly from the Laplace transform of the time dependent form of Maxwell's equations.

$$R = |r-r'| = [\rho^2 + \rho'^2 - 2\rho\rho' \cos(\phi-\phi') + (z-z')^2]^{\frac{1}{2}} \qquad (2.4b)$$

The charge and current are related in the continuity equation:

$$\rho_s(\bar{r}) = -\text{div}_s\, \bar{J}(r)/s = -\nabla_s \cdot \bar{J}(\bar{r})/s \qquad (2.5)$$

The combination of (2.1) through (2.5), enables one to write an electric field integral equation that is enforceable on the body surface; thus obtaining the electric currents:

$$\hat{n} \times \bar{E}^{inc}(\bar{r}) = \hat{n} \times \left\{ \left(\frac{s\mu}{4\pi}\right) \iint_S \bar{J}(\bar{r}')\, G(\bar{r},\bar{r}')dS' \right. \qquad (2.6)$$

$$\left. -(\tfrac{1}{4\pi}s\varepsilon)\, \nabla \iint_S \nabla'_s \cdot \bar{J}(\bar{r}')\, G(\bar{r},\bar{r}')dS' \right\} r \in S$$

Equation (2.6) can be written in operator form as

$$\bar{E}_t^{inc}(t) = B_{11}(\bar{J}_t) + B_{12}(\bar{J}_\phi) \qquad (2.7a)$$

$$\bar{E}_t^{inc}(t) = B_{12}(\bar{J}_t) + B_{22}(\bar{J}_\phi) \qquad (2.7b)$$

where Bij is the appropriate integro-differential operator, and is identifiable from (2.6). It is more straightforward to obtain expressions for the incident electric field using the arc coordinates $(\hat{t},\hat{\phi})$ rather than the more obvious cylindrical coordinates $(\hat{\rho},\hat{\phi},\hat{z})$. After the complete expressions for the operators in (2.7) are written, the operators are then partitioned into cylindrical coordinate system operators.

It is desirable to express all of the quantities of (2.7) in terms of local arc coordinates $(\hat{t},\hat{\phi})$ on the body surface. An orthogonal triad of unit vectors $(\hat{n},\hat{\phi},\hat{t})$ can be associated with each coordinate point $(\hat{t},\hat{\phi})$, where $\hat{n}$, $\hat{\phi}$, and $\hat{t}$ are defined as follows:

$$\hat{n} = \cos\gamma\cos\phi\,\hat{x} + \cos\gamma\sin\phi\,\hat{y} - \sin\gamma\,\hat{z} \tag{2.8a}$$

$$\hat{\phi} = -\sin\phi\,\hat{x} + \cos\phi\,\hat{y} \tag{2.8b}$$

$$\hat{z} = \sin\gamma\cos\phi\,\hat{x} + \sin\gamma\sin\phi\,\hat{y} + \cos\gamma\,\hat{z} \tag{2.8c}$$

γ is the angle between the tangent to the generating curve t, and the z-axis; defined to be positive if t points away from the z-axis, and negative if t points toward the z-axis. In this coordinate system, the surface divergence becomes

$$\nabla_s' \cdot \bar{J} = \frac{1}{\rho'}\frac{\partial}{\partial t'}(\rho'\bar{J}_t) + \frac{1}{\rho'}\frac{\partial}{\partial\phi'}(\bar{J}_\phi) \tag{2.9}$$

Expansion of (2.6) and comparison to (2.7) yields expressions for the Bij:

$$B_{11}(\bar{J}_t) = \frac{s\mu}{4\pi}\iint_S \bar{J}_t\,[\sin\gamma\sin\gamma'\cos(\phi-\phi') + \cos\gamma\cos\gamma']\;G\,dS'$$

$$-\frac{1}{4\pi s\varepsilon}\frac{\partial}{\partial t}\iint_S \frac{1}{\rho'}\frac{\partial}{\partial t'}(\rho'\,\bar{J}_t)\,G\,dS' \tag{2.10a}$$

$$B_{12}(\bar{J}_\phi) = \frac{-s\mu}{4\pi}\iint_S \bar{J}_\phi\sin\gamma\sin(\phi-\phi')\;G\,dS'$$

$$-\frac{1}{4\pi s\varepsilon}\frac{\partial}{\partial t}\iint_S \frac{1}{\rho'}\frac{\partial}{\partial\phi'}(\bar{J}_\phi)\,G\,dS' \tag{2.10b}$$

$$B_{21}(\bar{J}_t) = \frac{s\mu}{4\pi}\iint_S \bar{J}_t\sin\gamma'\sin(\phi-\phi')\;G\,dS'$$

$$-\frac{1}{4\pi s\rho\varepsilon}\frac{\partial}{\partial\phi}\iint_S \frac{1}{\rho'}\frac{\partial}{\partial t'}(\rho'\,\bar{J}_t)\,G\,dS' \tag{2.10c}$$

$$B_{22}(\bar{J}_\phi) = \frac{s\mu}{4\pi} \iint_S \bar{J}_\phi \cos(\phi-\phi')\, G\, dS'$$

$$- \frac{1}{4\pi s\rho\epsilon} \frac{\partial}{\partial\phi} \iint_S \frac{1}{\rho'} \frac{\partial}{\partial\phi'} (\bar{J}_\phi)\, G\, dS' \quad (2.10d)$$

A moment method scheme, also like that of Glisson and Wilton, was formulated to numerically solve (2.7). The generating arc is approximated by a sequence of linear segments, as shown in Figure 2, where the generating curve is assumed to lie in the $\phi = o$ plane. Rotation about the z-axis, of this segmented, generating arc, yields an approximation to the cylinder surface. The points $t_0, t_1, \ldots, t_{n+1}$ specify the end points of the linear segments that approximate the generating arc.

The unknown electric currents that are induced on the surface of the cylinder, can now be approximated by pulse functions in the t-direction, and are expanded in Fourier series in the ϕ-direction. The electric current expansion is given by

$$\bar{J}(t',\phi') \cong \frac{\hat{t}}{2\pi} \sum_{m=-\infty}^{\infty} \sum_{n=1}^{N} \bar{J}_t^{mn} P_1^n(t')\, e^{jm\phi'} \quad (2.11)$$

$$+ \frac{\hat{\phi}}{2\pi} \sum_{m=-\infty}^{\infty} \sum_{n=1}^{N+1} \bar{J}_\phi^{mn} P_2^n(t')\, e^{jm\phi'}$$

The charge contribution that comes from the derivative of J_t, with respect to t, can be approximated by

$$\frac{d}{dt}[\bar{J}_t(t',\phi')] = \frac{1}{2\pi} \sum_{m=-\infty}^{\infty} \sum_{n=1}^{N+1} \left(\frac{\bar{J}_t^{mn} - \bar{J}_t^{m,n-1}}{|t_n - t_{n-1}|} \right) P_2^n(t')\, e^{jm\phi} \quad (2.12)$$

and it is assumed that

$$\rho' \bar{J}_t^{m,0} \equiv \rho' \bar{J}_t^{m,n+1} \equiv 0 \quad (2.13)$$

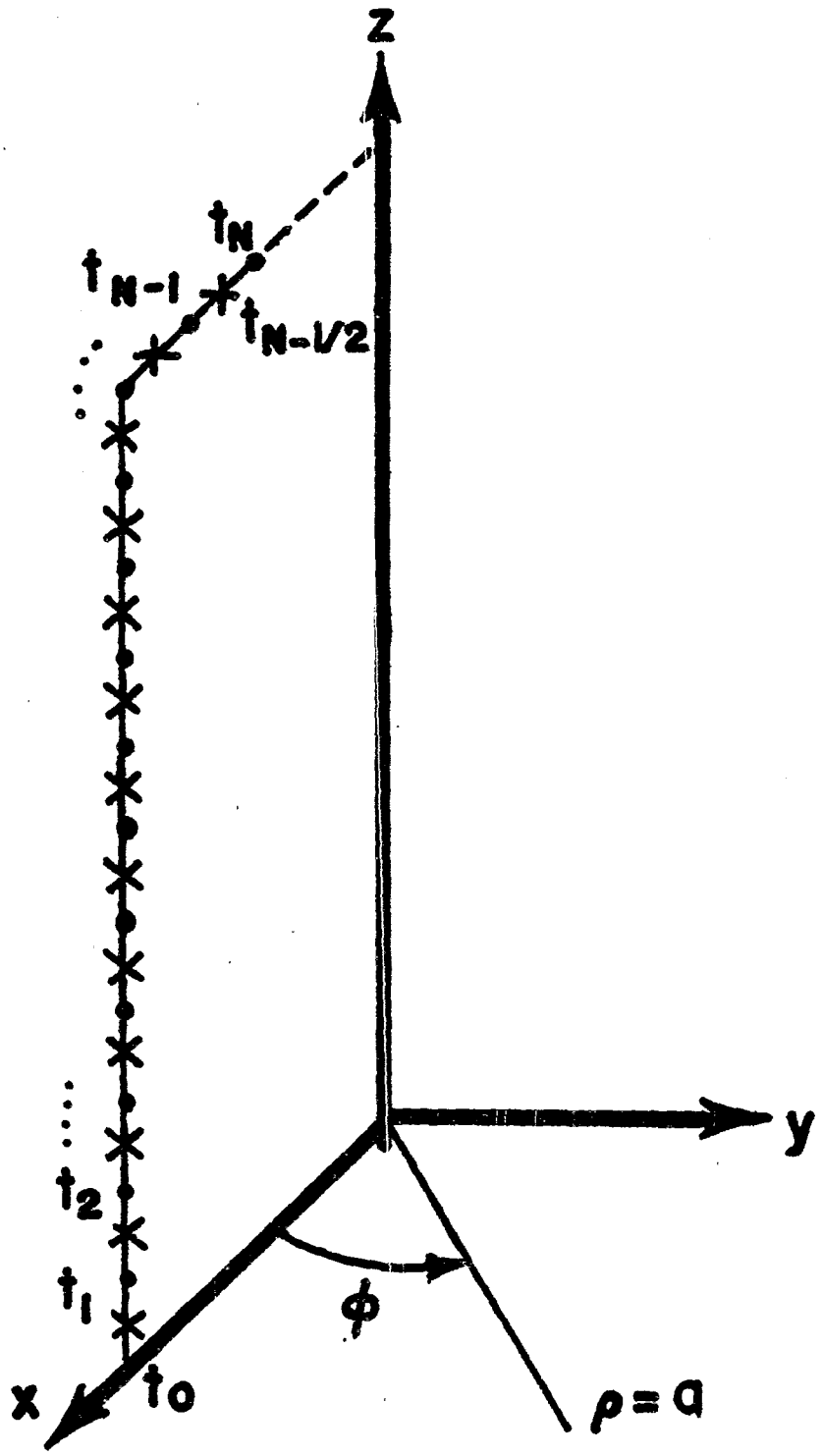

Figure 2. Segmentation of the generatrix for moment method numerical computations.

In the preceding,

$$P_1^n(t') = \begin{cases} 1, & t_{n-\frac{1}{2}} \leq t' \leq t_{n+\frac{1}{2}} \\ 0, & \text{otherwise} \end{cases} \tag{2.14a}$$

$$P_2^n(t') = \begin{cases} 1, & t_{n-1} \leq t' \leq t_n \\ 0, & \text{otherwise} \end{cases} \tag{2.14b}$$

$$|t_n - t_{n-1}| = [(\rho_n - \rho_{n-1})^2 + (z_n - z_{n-1})^2]^{\frac{1}{2}} \tag{2.15}$$

In fact, $\bar{J}_t(t', 0')$ is a generic representation of the current expansion. In $(\hat{\rho},\hat{\phi},\hat{z})$ coordinates, $\bar{J}_t(t',\phi')$ on the end cap, specializes to:

$$\bar{J}_t(t',\phi') = \rho'\bar{J}_\rho(\phi',z') \tag{2.16a}$$

and on the cylinder sidewall by:

$$\bar{J}_t(t',\phi') = \bar{J}_z(\phi',z') \tag{2.16b}$$

The first advantage of the expansion scheme (2.11) is that the Fourier components decouple, thus one can solve for an individual order of azimuthal variation. The expansion in (2.11) incorporates the "staggered zoning" scheme for the current and charge expansions. This staggered zoning method has been propounded by Wilton et. al. [10]. The staggered pulses basis approach has proven well suited

for use in numerical problems involving edges and two non-zero components of current. Details and features of this scheme are presented and discussed in [10] and [13].

The testing funcitons are defined as

$$T^q_{1m}(t) = \delta^q_{1m}(t) \tag{2.17a}$$

$$T^q_{2m}(t) = \delta^q_{2m}(t) \tag{2.17b}$$

where

$$\delta^q_{1m}(t) = \begin{cases} 1 & , t = t_q \\ 0 & , \text{otherwise} \end{cases} \tag{2.18a}$$

$$\delta^q_{2m}(t) = \begin{cases} 1 & , t = t_{q-\frac{1}{2}} \\ 0 & , \text{otherwise} \end{cases} \tag{2.18b}$$

Testing equation (2.7a) with (2.17a) and equation (2.7b) with (2.17b) yields

$$\bar{E}^{inc}_{tm}(t_q) = B^{qn}_{11m}(\bar{J}_{tm}) + B^{qn}_{12m}(\bar{J}_{\phi m}) \tag{2.19a}$$

$$\bar{E}^{inc}_{\phi m}(t_q) = B^{qn}_{21m}(\bar{J}_{tm}) + B^{qn}_{22m}(\bar{J}_{\phi m}) \tag{2.19b}$$

The generalized impedance matrix, that consists of the B_{ijm}, can be written explicitly. The subscript m refers to the Fourier coefficient, and the q and n superscripts refer to field and observation points respectively. For convenience in writing these expressions, two frequently used integrals will be denoted as follows

$$K(t_1,t_2;t_q,m) = \int_{t_1}^{t_2} G_m(t_q,t')dt' \qquad (2.20a)$$

$$K^{\rho}(t_1,t_2;t_q,m) = \int_{t_1}^{t_2} G_m(t_q,t')\rho' dt' \qquad (2.20b)$$

where G_m is defined by equation (2.4a). Auxiliary "weight" functions that arise from testing in the t-direction are introduced:

$$\chi_s(\Delta t_q,\gamma_q) = (\Delta t_{q+1} \sin \gamma_{q+1} + \Delta t_q \sin \gamma_q)/2 \qquad (2.21a)$$

$$\chi_c(\Delta t_q,\gamma_q) = (\Delta t_{q+1} \cos \gamma_{q+1} + \Delta t_q \cos \gamma_q)/2 \qquad (2.21b)$$

The operators in (2.7) can now be expressed as:

$$B_{11m}^{qn} = \frac{s\mu}{8\pi} \sin \gamma_{n+1} \chi_s(\Delta t_q,\gamma_q)[K(t_{n-\frac{1}{2}},t_n;\ t_q,m+1) + K(t_{n-\frac{1}{2}},t_n;\ t_q,m-1)]$$

$$+ \frac{s\mu}{8\pi} \sin \gamma_{n+1} \chi_s(\Delta t_q,\gamma_q)[K(t_n,t_{n+\frac{1}{2}};\ t_q,m+1) + K(t_n,t_{n+\frac{1}{2}};\ t_q,m-1)]$$

$$+ \frac{s\mu}{4\pi} \cos \gamma_n \chi_c(\Delta t_q,\gamma_q)\ K\ (t_{n-\frac{1}{2}},t_n;\ t_q,m)$$

$$+ \frac{s\mu}{4\pi} \cos \gamma_{n+1} \chi_c(\Delta t_q,\ \gamma_q)\ K\ (t_n,t_{n+\frac{1}{2}};\ t_q,m)$$

$$- \frac{1}{4\pi s\varepsilon \Delta t_n}\ [K^{\rho}(t_{n-1},t_n;\ t_{q+\frac{1}{2}},m) - K^{\rho}(t_{n-1},t_n;\ t_{q-\frac{1}{2}},m)]$$

$$+ \frac{1}{4\pi s\varepsilon \Delta t_{n+1}} [K^{\rho}(t_n, t_{n+1};\ t_{q+\frac{1}{2}}, m) - K^{\rho}(t_n, t_{n+1};\ t_{q-\frac{1}{2}}, m)] \tag{2.22a}$$

$$B_{12}^{qn} = \frac{js\mu}{8\pi} \chi_s(\Delta t_q, \gamma_q)[K^{\rho}(t_{n-1}, t_n;\ t_q, m+1) - K^{\rho}(t_{n-1}, t_n;\ t_q, m-1)]$$

$$- \frac{jm}{4\pi s\varepsilon} [K(t_{n-1}, t_n;\ t_{q+\frac{1}{2}}, m) - K(t_{n-1}, t_n;\ t_{q-\frac{1}{2}}, m)] \tag{2.22b}$$

$$B_{21}^{qn} = \frac{-js\mu}{8\pi} \Delta t_q \sin \gamma_n [K(t_{n-\frac{1}{2}}, t_n;\ t_{q-\frac{1}{2}}, m+1) - K(t_{n-\frac{1}{2}}, t_n;\ t_{q-\frac{1}{2}}, m-1)]$$

$$- \frac{js\mu}{8\pi} \Delta t_q \sin \gamma_{n+1} [K(t_n, t_{n+\frac{1}{2}};\ t_{q-\frac{1}{2}}, m+1) - K(t_n, t_{n+\frac{1}{2}};\ t_{q-\frac{1}{2}}, m-1)]$$

$$- \frac{jm\Delta t_q}{4\pi s\rho_{q-\frac{1}{2}}\varepsilon \Delta t_n} K(t_{n-1}, t_n;\ t_{q-\frac{1}{2}}, m)$$

$$+ \frac{jm\Delta t_q}{4\pi s\rho_{q-\frac{1}{2}}\varepsilon \Delta t_{n+1}} K(t_n, t_{n+1};\ t_{q-\frac{1}{2}}, m) \tag{2.22c}$$

$$B_{22m}^{qn} = \frac{s\mu\Delta t_q}{8\pi} [K^{\rho}(t_{n-1}, t_n;\ t_{q-\frac{1}{2}}, m+1) + K^{\rho}(t_{n-1}, t_n;\ t_{q-\frac{1}{2}}, m-1)]$$

$$+ \frac{m^2\Delta t_q}{4\pi s\rho_{q-\frac{1}{2}}\varepsilon} K(t_{n-1}, t_n;\ t_{q+\frac{1}{2}}, m) \tag{2.22d}$$

Now, if (2.7) is particularized to $(\hat{\rho}, \hat{\phi}, \hat{z})$ coordinates, E_t, E_ϕ, J_t and J_ϕ each have two components: E_z^c and $E_\rho^{\mathcal{C}}$, E_ϕ^c and $E_\phi^{\mathcal{C}}$, J_z^c and $J_\rho^{\mathcal{C}}$, and J_ϕ^c and $J_\phi^{\mathcal{C}}$ respectively. Script $\mathcal{C}$ denotes quantities on the endcap, while c denotes quantities on the sidewall. Splitting (2.7) into cap and sidewall components yields:

$$E_{\phi}^{c}(\rho) = A_{c\rho}^{cz}(J_z^c) + A_{c\rho}^{c\rho}(J_\rho^c) + A_{c\rho}^{c\phi}(J_\phi^c) + A_{c\phi}^{c\phi}(J_\phi^c) \qquad (2.23a)$$

$$E_{\phi}^{c}(z) = A_{c\phi}^{cz}(J_z^c) + A_{c\phi}^{c\rho}(J_\rho^c) + A_{c\phi}^{c\phi}(J_\phi^c) + A_{c\phi}^{c\phi}(J_\phi^c) \qquad (2.23b)$$

$$E_{\rho}^{c}(\rho) = A_{c\rho}^{cz}(J_z^c) + A_{c\rho}^{c\rho}(J_\rho^c) + A_{c\rho}^{c\phi}(J_\phi^c) + A_{c\phi}^{c\phi}(J_\phi^c) \qquad (2.23c)$$

$$E_{z}^{c}(z) = A_{cz}^{cz}(J_z^c) + A_{cz}^{c\rho}(J_\rho^c) + A_{cz}^{c\phi}(J_\phi^c) + A_{cz}^{c\phi}(J_\phi^c) \qquad (2.23d)$$

where the upper superscript of the operator indicates the current location (cap or sidewall) and direction ($\hat{\rho},\hat{\phi},\hat{z}$), and the lower superscript indicates the field location and direction. Recall from the definition of γ that $\gamma=0$ on the sidewall, and that $\gamma=-\rho/2$ on the cylinder cap. The natural modes on the structure can be partitioned into two symmetry classes—one associated with a magnetic symmetry plane and the other with an electric image plane. Symmetry allows a significant reduction in the number of unknowns to be found in this problem. Using these symmetry properties and the previous definitions, the operators in Eq.(2.23) can be identified from Eq.(2.22). This identification obtains the following sixteen submatrix forms resulting from each of four field components computed from the four current source components:

$$A_m^{cz\,qn} = \frac{sa\mu\Delta_z}{4\pi}\left[K^{+}(Z_{n-\frac{1}{2}},Z_{n+\frac{1}{2}};\ Z_q,m) \pm K^{-}(Z_{n-\frac{1}{2}},Z_{n+\frac{1}{2}};\ Z_q,m)\right]$$

$$- \frac{a}{4\pi s\varepsilon\Delta_z}\Big\{\left[K^{+}(Z_{n-1},Z_n;\ Z_{q+\frac{1}{2}},m) \mp K^{-}(Z_{n-1},Z_n;\ Z_{q+\frac{1}{2}},m)\right]$$

$$- \left[K^{+}(Z_n,Z_{n+1};\ Z_{q+\frac{1}{2}},m) \mp K^{-}(Z_n,Z_{n+1};\ Z_{q+\frac{1}{2}},m)\right]$$

$$- [K^{+}(Z_{n-1},Z_n;\ Z_{q-\frac{1}{2}},m) \mp K^{-}(Z_{n-1},Z_n;\ Z_{q-\frac{1}{2}},m)]$$
$$+ [K^{+}(Z_n,Z_{n+1};\ Z_{q-\frac{1}{2}},m) \mp K^{-}(Z_n,Z_{n+1};\ Z_{q-\frac{1}{2}},m)] \Big\} \quad (2.24a)$$

$$A_m^{c\rho}{}_{cz}{}_{qn} = - \frac{1}{4\pi s\varepsilon\Delta_\rho} [K^{+}(\rho_{n-1},\rho_n;\ Z_{q+\frac{1}{2}},m) \mp K^{-}(\rho_{n-1},\rho_n;\ Z_{q+\frac{1}{2}},m)]$$
$$+ \frac{1}{4\pi s\varepsilon\Delta_\rho} [K^{+}(\rho_n,\rho_{n+1};\ Z_{q+\frac{1}{2}},m) \mp K^{-}(\rho_n,\rho_{n+1};\ Z_{q+\frac{1}{2}},m)]$$
$$+ \frac{1}{4\pi s\varepsilon\Delta_\rho} [K^{+}(\rho_{n-1},\rho_n;\ Z_{q-\frac{1}{2}},m) \mp K^{-}(\rho_{n-1},\rho_n;\ Z_{q-\frac{1}{2}},m)]$$
$$- \frac{1}{4\pi s\varepsilon\Delta_\rho} [K^{+}(\rho_n,\rho_{n+1};\ Z_{q-\frac{1}{2}},m) \mp K^{-}(\rho_n,\rho_{n+1};\ Z_{q-\frac{1}{2}},m)] \quad (2.24b)$$

$$A_m^{c\phi}{}_{cz}{}_{qn} = - \frac{mj}{4\pi s\varepsilon} [K^{+}(Z_{n-1},Z_n;\ Z_{q+\frac{1}{2}},m) \mp K^{-}(Z_{n-1},Z_n;\ Z_{q-\frac{1}{2}},m)] \quad (2.24c)$$

$$A_m^{c\phi}{}_{c\rho}{}_{qn} = - \frac{j}{4\pi s\varepsilon} [K^{+}(\rho_{n-1},\rho_n;\ Z_{q+\frac{1}{2}},m) \mp K^{-}(\rho_{n-1},\rho_n;\ Z_{q+\frac{1}{2}},m)]$$
$$+ \frac{j}{4\pi s\varepsilon} [K^{+}(\rho_{n-1},\rho_n;\ Z_{q-\frac{1}{2}},m) \mp K^{-}(\rho_{n-1},\rho_n;\ Z_{q-\frac{1}{2}},m)] \quad (2.24d)$$

$$A_m^{cz}{}_{c\rho}{}_{qn} = - \frac{a}{4\pi s\varepsilon\Delta_\rho} [K^{+}(Z_{n-1},Z_n;\rho_{q+\frac{1}{2}},m) \mp K^{-}(Z_{n-1},Z_n;\rho_{q+\frac{1}{2}},m)]$$
$$+ \frac{a}{4\pi s\varepsilon\Delta_\rho} [K^{+}(Z_{n-1},Z_n;\ \rho_{q-\frac{1}{2}},m) \mp K(Z_{n-1},Z_n;\ \rho_{q-\frac{1}{2}},m)]$$
$$+ \frac{a}{4\pi s\varepsilon\Delta_\rho} [K^{+}(Z_n,Z_{n+1};\ \rho_{q+\frac{1}{2}},m) \mp K^{-}(Z_n,Z_{n+1};\ \rho_{q+\frac{1}{2}},m)]$$
$$- \frac{a}{4\pi s\varepsilon\Delta_\rho} [K^{+}(Z_n,Z_{n+1};\ \rho_{q-\frac{1}{2}},m) \mp K^{-}(Z_n,Z_{n+1};\ \rho_{q-\frac{1}{2}},m)] \quad (2.24e)$$

$$A_m^{\xi\rho qn} = -\frac{s\mu\Delta_\rho}{8\pi}\,[K^+(\rho_{n-\frac{1}{2}},\rho_{n+\frac{1}{2}};\ \rho_q,m+1)$$

$$\mp K^-(\rho_{n-\frac{1}{2}},\rho_{n+\frac{1}{2}};\ \rho_q,m+1)$$

$$+ K^+(\rho_{n-\frac{1}{2}},\rho_{n+\frac{1}{2}};\ \rho_q,m-1)$$

$$\mp K^-(\rho_{n-\frac{1}{2}},\rho_{n+\frac{1}{2}};\ \rho_q,m-1)]$$

$$-\frac{1}{4\pi s\epsilon\Delta_\rho}\Big\{[K^+(\rho_{n-1},\rho_n;\ \rho_{q+\frac{1}{2}},m)$$

$$\mp K^-(\rho_{n-1},\rho_n;\ \rho_{q+\frac{1}{2}},m)]$$

$$-[K^+(\rho_{n-1},\rho_n;\ \rho_{q-\frac{1}{2}},m)$$

$$\mp K^-(p_{n-1},p_n;\ p_{q-\frac{1}{2}},m)]\Big\}$$

$$+\frac{1}{4\pi s\epsilon\Delta_\rho}\Big\{[K^+(\rho_n,\rho_{n+1};\ \rho_{q+\frac{1}{2}},m)$$

$$\mp K^-(\rho_n,\rho_{n+1};\ \rho_{q+\frac{1}{2}},m)]$$

$$-[K^+(\rho_n,\rho_{n+1};\ \rho_{q-\frac{1}{2}},m)$$

$$\mp K^-(\rho_n,\rho_{n+1};\ \rho_{q-\frac{1}{2}},m)]\Big\} \qquad (2.24f)$$

$$A_m^{\xi\phi qn} = \frac{js\mu}{8\pi}\Big\{[K^{\rho+}(Z_{n-1},Z_n;\ \rho_q,m+1)$$

$$\mp K^{\rho-}(Z_{n-1},Z_n;\ \rho_q,m+1)]$$

$$-[K^{\rho+}(Z_{n-1},Z_n;\ \rho_q,m-1)$$

$$\mp K^{\rho-}(Z_{n-1},Z_n;\ \rho_q,m-1)]\Big\}$$

$$-\frac{j}{4\pi s\epsilon}\Big\{[K^+(Z_{n-1},Z_n;\ \rho_{q+\frac{1}{2}},m)$$

$$\mp K^-(Z_{n-1},\ Z_n;\ \rho_{q+\frac{1}{2}},m)]$$

$$-[K^+(Z_{n-1},Z_n;\ \rho_{q-\frac{1}{2}},m)$$

$$\mp K^-(Z_{n-1},Z_n;\ \rho_{q-\frac{1}{2}},m)]\Big\} \qquad (2.24g)$$

$$A_m^{c\phi}{}_{c\rho qn} = \frac{js\mu\Delta_\rho}{8\pi}\left\{[K^{\rho+}(\rho_{n-1},\rho_n;\ \rho_q,m+1) \mp K^{\rho-}(\rho_{n-1},\rho_n;\ \rho_q,m+1)]\right.$$

$$\left. - [K^{\rho+}(\rho_{n-1},\rho_n;\ \rho_q,m-1) \mp K^{\rho-}(\rho_{n-1},\rho_n;\ \rho_q,m-1)]\right\}$$

$$- \frac{j}{4\pi s\varepsilon}\left\{[K^{+}(\rho_{n-1},\rho_n;\ \rho_{q+\frac{1}{2}},m) \mp K^{-}(\rho_{n-1},\rho_n;\ \rho_{q+\frac{1}{2}},m)]\right.$$

$$\left. - [K^{+}(\rho_{n-1},\rho_n;\ \rho_{q-\frac{1}{2}},m) \mp K^{-}(\rho_{n-1},\rho_n;\ \rho_{q-\frac{1}{2}},m)]\right\} \qquad (2.24h)$$

$$A_m^{cz}{}_{c\phi qn} = -\frac{jm}{4\pi s\varepsilon}\,[K^{+}(Z_{n-1},Z_n;\ \rho_{q-\frac{1}{2}},m) \mp K^{-}(Z_{n-1},Z_n;\ \rho_{q-\frac{1}{2}},m)]$$

$$+ \frac{jm}{4\pi s\varepsilon}\,[K^{+}(Z_n,Z_{n+1};\ Z_{q-\frac{1}{2}},m) \mp K^{-}(Z_n,Z_{n+1};\ Z_{q-\frac{1}{2}},m)] \qquad (2.24i)$$

$$A_m^{c\rho}{}_{c\phi qn} = -\frac{js\mu\Delta_z}{8\pi}\left\{[K^{+}(\rho_{n-\frac{1}{2}},\rho_{n+\frac{1}{2}};\ Z_{q-\frac{1}{2}},m+1) \mp K^{-}(\rho_{n-\frac{1}{2}},\rho_{n+\frac{1}{2}};\ Z_{q-\frac{1}{2}},m+1)]\right.$$

$$\left. - [K^{+}(\rho_{n-\frac{1}{2}},\rho_{n+\frac{1}{2}};\ Z_{q-\frac{1}{2}},m-1) \mp K^{-}(\rho_{n-\frac{1}{2}},\rho_{n+\frac{1}{2}};\ Z_{q-\frac{1}{2}},m-1)]\right.$$

$$- \frac{jm\Delta_z}{4\pi s\varepsilon a\Delta_\rho}\left\{K^{+}(\rho_{n-1},\rho_n;\ Z_{q-\frac{1}{2}},m) \mp K^{-}(\rho_{n-1},\rho_n;\ Z_{q-\frac{1}{2}},m)\right.$$

$$\left. - [K^{+}(\rho_n,\rho_{n+1};\ Z_{q-\frac{1}{2}},m) \mp K^{-}(\rho_n,\rho_{n+1};\ Z_{q-\frac{1}{2}},m)]\right\} \qquad (2.24j)$$

$$A_m^{c\phi}{}_{c\phi qn} = \frac{s\mu a\Delta_z}{8\pi}\left\{[K^{+}(Z_{n-1},Z_n;\ Z_{q-\frac{1}{2}},m+1) \mp K^{-}(Z_{n-1},Z_n;\ Z_{q-\frac{1}{2}},m+1)]\right.$$

$$\left. + [K^{+}(Z_{n-1},Z_n;\ Z_{q-\frac{1}{2}},m-1) \mp K^{-}(Z_{n-1},Z_n;\ Z_{q-\frac{1}{2}},m-1)]\right\}$$

$$+ \frac{m^2\Delta_z}{4\pi sa\varepsilon}\,[K^{+}(Z_{n-1},Z_n;\ Z_{q-\frac{1}{2}},m) \mp K^{-}(Z_{n-1},Z_n;\ Z_{q-\frac{1}{2}},m)] \qquad (2.24k)$$

$$A_m^{c\phi qn} = \frac{s\mu\Delta_z}{8\pi}\left[K^{\rho+}(\rho_{n-1},\rho_n;\ Z_{q-\frac{1}{2}},m+1) \mp K^{\rho-}(\rho_{n-1},\rho_n;\ Z_{q-\frac{1}{2}},m+1)\right.$$

$$\left. + K^{\rho}(\rho_{n-1},\rho_n;\ Z_{q-\frac{1}{2}},m-1) \mp K^{\rho-}(\rho_{n-1},\rho_n;\ Z_{q-\frac{1}{2}},m-1)\right]$$

$$+ \frac{m^2\Delta_z}{4\pi s\varepsilon a}\left[K^{+}(\rho_{n-1},\rho_n;\ Z_{q-\frac{1}{2}},m) \mp K^{-}(\rho_{n-1},\rho_n;\ Z_{q-\frac{1}{2}},m)\right] \qquad (2.241)$$

$$A_m^{cqn} = -\frac{jm\Delta_\rho a}{4\pi s\varepsilon\Delta_z\rho_{q-\frac{1}{2}}}\left\{\left[K^{+}(Z_{n-1},Z_n;\ \rho_{q-\frac{1}{2}},m) \mp K^{-}(Z_{n-1},Z_n;\ \rho_{q-\frac{1}{2}},m)\right]\right.$$

$$\left. - \left[K^{+}(Z_n,Z_{n+1};\ \rho_{q-\frac{1}{2}},m) \mp K^{-}(Z_n,Z_{n+1};\ \rho_{q-\frac{1}{2}},m)\right]\right\} \qquad (2.24m)$$

$$A_m^{c\phi qn} = \frac{js\mu\Delta_\rho}{8\pi}\left\{\left[K^{+}(\rho_{n-\frac{1}{2}},\rho_{n+\frac{1}{2}};\ \rho_{q-\frac{1}{2}},m+1) \mp K^{-}(\rho_{n-\frac{1}{2}},\rho_{n+\frac{1}{2}};\ \rho_{q-\frac{1}{2}},m+1)\right]\right.$$

$$\left. - \left[K^{+}(\rho_{n-\frac{1}{2}},\rho_{n+\frac{1}{2}};\ \rho_{q-\frac{1}{2}},m-1) \mp K^{-}(\rho_{n-\frac{1}{2}},\rho_{n+\frac{1}{2}};\ \rho_{q-\frac{1}{2}},m-1)\right]\right\}$$

$$- \frac{jm}{4\pi s\varepsilon\rho_{q-\frac{1}{2}}}\left[K^{+}(\rho_{n-1},\rho_n;\ \rho_{q-\frac{1}{2}},m) \mp K^{-}(\rho_{n-1},\rho_n;\ \rho_{q-\frac{1}{2}},m)\right]$$

$$- \frac{jm}{4\pi s\varepsilon\rho_{q-\frac{1}{2}}}\left[K^{+}(\rho_n,\rho_{n+1};\ \rho_{q-\frac{1}{2}},m) \mp K^{-}(\rho_n,\rho_{n+1};\ \rho_{q-\frac{1}{2}},m)\right] \qquad (2.24n)$$

$$A_m^{\phi qn} = \frac{s\mu\Delta_\rho a}{8\pi}\left\{\left[K^{+}(Z_{n-1},Z_n;\ \rho_{q-\frac{1}{2}},m+1) \mp K^{-}(Z_{n-1},Z_n;\ \rho_{q-\frac{1}{2}},m+1)\right]\right.$$

$$\left. + \left[K^{+}(Z_{n-1},Z_n;\ \rho_{q-\frac{1}{2}},m-1) \mp K^{-}(Z_{n-1},Z_n;\ \rho_{q-\frac{1}{2}},m-1)\right]\right\}$$

$$+ \frac{m^2\Delta_\rho}{4\pi s\varepsilon\rho_{q-\frac{1}{2}}}\left[K^{+}(Z_{n-1},Z_n;\ \rho_{q-\frac{1}{2}},m) \mp K^{-}(Z_{n-1},Z_n;\ \rho_{q-\frac{1}{2}},m)\right] \qquad (2.24o)$$

$$A_m^{c\phi qn} = \frac{s\mu\Delta_\rho}{8\pi}\left\{[K^{\rho+}(\rho_{n-1},\rho_n;\ \rho_{q-\frac{1}{2}},m+1) \mp K^{\rho-}(\rho_{n-1},\rho_n;\ \rho_{q-\frac{1}{2}},m+1)]\right.$$
$$\left. + [K^{\rho+}(\rho_{n-1},\rho_n;\ \rho_{q-\frac{1}{2}},m-1) \mp K^{\rho-}(\rho_{n-1},\rho_n;\ \rho_{q-\frac{1}{2}},m-1)]\right\}$$
$$+ \frac{m^2\Delta_\rho}{4\pi s\varepsilon\rho_{q-\frac{1}{2}}}[K^{+}(\rho_{n-1},\rho_n;\ \rho_{q-\frac{1}{2}},m) \mp K^{-}(\rho_{n-1},\rho_n;\ \rho_{q-\frac{1}{2}},m)] \quad (2.24p)$$

In the preceding equations, Z_j and ρ_j can be interpreted as $t_j = (Z_j,\rho_j)$. The + and - superscripts indicate integrals on the upper half-cylinder and on the image half-cylinder, respectively. The upper signs refer to the electric image plane, while the lower signs indicate the magnetic image plane. The singularity that occurs in the self-case, that is, when the source and observation point coincide, is dealt with in two fashions. In the case of A^{cz}_{cz}, $A^{c\phi}_{cz}$, $A^{cz}_{c\phi}$, $A^{c\phi}_{c\phi}$, the singularity was treated as by Melson, [8]; in the case of the other operators, the singularity was handled as in Glisson and Wilton [10].

2.3 SEM Characterization

For subsequent interpretative purposes, Eq.(2.19) is written in dyadic operator form

$$< \bar{\bar{\Gamma}}(\bar{r},\bar{r}'s);\ \bar{J}(\bar{r}) > = \tan\left\{\bar{E}^{inc}(\bar{r},s)\right\} \qquad \bar{r} \in S \quad (2.25)$$

where <;> denotes a symmetric product, defined as

$$< \bar{\bar{F}}\ ;\ \bar{G} > = \iint_S \bar{\bar{F}} \cdot \bar{G}\, dS \quad (2.26)$$

The operator statement of the integral equation (2.25) constitutes a complete electromagnetic description of the given scatterer. Consequently, the operator G has associated with it, all of the SEM

poles for the structure. Equation (2.25) exhibits the complete decoupling of the Fourier harmonic modes; hence, it allows the determination of each harmonic, current mode independently. This fact is of paramount importance in the SEM parameter determination because decoupling naturally partitions the SEM data into disjoint sets, each associated with a particular harmonic mode: m=0,1,2,... . Only a finite collection data is desired for only a few modes.

The SEM representation for the surface current on the closed cylinder proceeds from (2.25). The integral equations (2.25) possess homogeneous solutions of a collection of complex frequencies (s_{mi}) for which G is singular—the complex natural resonances, or poles, associated with the mth harmonic. Viz.,

$$< \bar{\bar{\Gamma}}_m(\bar{r},\bar{r}',s_{mi}) \; ; \; \bar{J}_{mi}(\bar{r}) > = 0 \qquad (2.27)$$

The associated homogeneous solutions $\bar{J}_{mi}(r)$ of (2.27) are termed the natural modes. Clearly, the modes and poles are associated through the indices mi. The determination and physical interpretation of these quantities is the primary purpose of this work. The numerical procedure applied to (2.25) is discussed in Section 2.

In the frequency domain, the SEM expansion for the induced surface current $\bar{J}$ is, as described by Tesche [6],

$$\bar{J}(\bar{r},s) = \sum_n \sum_i \beta_{mi} \, \eta_{mi} \, \bar{J}_{mi}(\bar{r}) \; (1/(s-s_{mi}) + 1/s_{mi}) \qquad (2.28a)$$

where β_{mi} is the SEM normalization constant defined by

$$\beta_{mi} = < \bar{J}_{mi}(\bar{r}'); \frac{\partial}{\partial s} (\bar{\bar{\Gamma}}(\bar{r},\bar{r}',s_{mi})); \bar{J}_{mi}(\bar{r}') >^{-1} \qquad (2.28b)$$

and where η_{mi} is an SEM coupling coefficient defined by

$$\eta_{mi} = < \bar{J}_{mi}(\bar{r},s_{mi}) \; ; \; \bar{E}^{inc}(\bar{r},s_{mi}) > \qquad (2.28c)$$

Solutions to Eq. (2.27), which is itself a harmonic-by-harmonic, tensor statement of Eq. (2.7), are also solutions to Eq.(2.7). Poles and natural modes of Eq.(2.27) are, therefore, poles and natural modes of Eq.(2.7).

The integral equation (2.19) can be approximated by a square system of algebraic equations through application of the numerical technique described in Section 2.2,

$$[Z_m(s_{mi})]\ [J_m(s_{mi})] = [V_m(s_{mi})] \qquad (2.29)$$

where $[Z_m(s)]$ and $[V_m(s)]$ are the response and source vectors respectively. To solve for the natural resonant frequencies, that is, where the incident E-field is zero, Eq.(2.29) becomes:

$$[Z_m(s_{mi})]\ [J_{mi}] = 0 \qquad (2.30)$$

yielding s_{mi}. These s_{mi} are numerical approximations to the resonant frequencies. For (2.30) to have a non-trivial solution, the determinant of $[Z_m(s)]$ must vanish at these frequencies. Therefore to determine the natural resonances of the current for the closed cylinder, the equation

$$\det[Z_m(s_{mi})] = 0 \qquad (2.31)$$

must be solved. When the equation above was constructed (see Section 2), symmetry was invoked, not only to reduce the number of unknowns in the problem, but also to allow location of both "even" and "odd" poles for a given harmonic mode. Solving the

BOR problem of a whole cylinder yields only the even poles, those corresponding to an electric image plane. Notice, that Eq.(2.28) requires the SEM parameters belonging to both kinds of poles. Use of symmetry planes to obtain both classes of poles has been discussed by Baum in [14].

Considerable knowledge about the location and nature of the natural frequencies can be inferred from (2.31); from the analogy to circuit theory, as Tesche [6] points out; and from the location of the natural frequencies of the open cylinder. Because the time domain current is real, the poles must either occur in conjugate pairs or be real. From circuit theory, it is observed that the resonances must lie in the left-half of the s-plane, since the time behavior of the current is as exp(st), and since, an exponentially growing current is not physically possible on a passive scatterer. Furthermore, closed cylinder poles should lie "near" corresponding open cylinder poles—at least for the large aspect ratio cylinders (recall: large aspect ratio implies thin cylinder): for thin cylinders any endcap effects should be small.

Since the natural resonances of the current are determined from the zeros of the determinant of the impedance matrix, a zero finding procedure such as Muller's method [15] was implemented. An exhaustive search method such as the contour method of Singaraju et. al. [16], was undesirable, and unneccessary for the brunt of the computations in this application. Such a search procedure would have required vastly more computer time than what was, in fact, used. The exhaustive search procedure was unneccessary because the Muller method search always either converged to a pole

or terminated itself upon reaching the imaginary axis. In the initial stages of the computations, the contour method was, in fact, employed. The data obtained corroborated that the closed cylinder poles correspond to those of the open cylinder (obtained by Melson [8]) on a one-to-one basis. Iterative search based on the presumption of one-to-one correspondence was used subsequently and none of the several hundred iterations conducted converged to a pole location contradicting this presumption.

The current existing for a zero forcing funtion at a singular point s_{mi}, has been called a current natural mode $[J_{mi}]$; a current natural mode is a solution to Eq.(2.30). Therefore, to obtain the current natural mode, the homogeneous solution of (2.29) must be found. This homogeneous solution, $[J_{tmi}(t)]$, is, in general, a complex quantity having an arbitrary magnitude. To be consistent with the natural modes for the open cylinder that were reported by Melson, those current natural modes having no azimuthal variation, are normalized on a peak value basis, while the higher order modes have been normalized with respect to the magnitude of the symmetric product of a mode with itself.

The symmetric product is defined in (2.26) as

$$< \overline{F};\overline{G} > = \iint \overline{F} \cdot \overline{G}\, dS \qquad (2.32)$$

where S is the surface of the closed cylinder. Again, as in the formulation, it is expedient to use $(\hat{t},\hat{\phi})$ coordinates for awhile. The two components of current can be defined as

$$J_{tmi}(\phi,t) = \frac{1}{\pi} J_{tmi}(t) \cos m\phi \qquad (2.33a)$$

$$J_{\phi mi}(\phi,t) = \frac{j}{\pi} J_{\phi mi}(t) \sin m\phi \qquad (2.33b)$$

Substituting (2.33a) and (2.33b) into (2.32), and specializing the surface integration to the body of a closed cylinder, equation (2.32) becomes

$$< \bar{J}_{mi} ; \bar{J}_{mi} > = \frac{1}{\pi} \int_{-t_o}^{t_o} [J^2_{tmi}(t) - J^2_{\phi mi}(t)]\rho \, dt \qquad (2.34)$$

Equation (2.34) written in cylindrical coordinates, is

$$\begin{aligned} < \bar{J}_{mi} ; \bar{J}_{mi} > = & \int_{(a_o,-h)}^{(a,-h)} [J^2_{\rho mi}(\rho_1) - J^2_{\phi mi}(\rho_1)]\rho \, d\rho_1 \\ & + \frac{a}{\pi} \int_{-h}^{h} [J^2_{zmi}(z) - J^2_{\phi mi}(z)]dz \\ & + \frac{1}{\pi} \int_{(a,h)}^{(a_o h)} [J^2_{\rho mi}(\rho_z) - J^2_{\phi mi}(\rho_z)]\rho_z \, d\rho_z \end{aligned} \qquad (2.35)$$

This simplifies to

$$\begin{aligned} < \bar{J}_{mi} ; \bar{J}_{mi} > = & \frac{a}{\pi} \int_{-h}^{h} [J^2_{zmi}(z) - J^2_{\phi mi}(z)]dz \\ & + \frac{2}{\pi} \int_{a}^{a_o} [J^2_{\rho mi}(\rho) - J^2_{\phi mi}(\rho)] \, d \end{aligned} \qquad (2.36)$$

Now, letting $Z = 2h\zeta$ and $p = 2h\xi$, and using the definition of aspect ratio,

$$\alpha = h/a = h/2a \qquad (2.37)$$

where h is the half-length, L is the length, and a is the outer radius, of the cylinder, Eq.(2.36) can be rewritten as:

$$< \bar{J}_{mi} ; \bar{J}_{mi} > = \frac{La}{\pi} \int_{-0.5}^{0.5} [J^2_{zmi}(\zeta L) - J^2_{\phi mi}(\zeta L)]d\zeta$$

$$+ \frac{2L^2}{\pi^2} \int_{\frac{1}{2}\alpha}^{2a} {}_{o}^{\alpha} \left[\frac{(\xi J_{\rho mi}(L\xi))^2}{\xi} - \xi J_{\phi m}(L\xi) \right] d\xi \tag{2.38}$$

The surface area, S of the cylinder sidewall is

$$S = 2\pi aL = \pi L^2/\alpha \tag{2.39}$$

Substitution of (2.39) into (2.38) gives,

$$< J_{mi} ; J_{mi} > = S \left\{ \frac{1}{2\pi^2} \int_{-0.5}^{0.5} [J^2_{zmi}(\zeta L) + J^2_{\phi mi}(\zeta L)]d\zeta \right.$$

$$\left. - \frac{2\alpha}{\pi^2} \int_{\frac{1}{2}\alpha}^{2\alpha a} {}_{o} \left[\frac{(\xi J_{\rho mi}(\xi L))^2}{\xi} - \xi J^2_{\phi mi} \right] d\xi \right\} \tag{2.40}$$

Choosing

$$\frac{1}{2\pi^2} \int_{-0.5}^{0.5} [J^2_{zmi}(\zeta L) + J^2_{\phi mi}(\zeta L)]d\zeta$$

$$- \frac{2\alpha}{\pi^2} \int_{\frac{1}{2}\alpha}^{2\alpha a} {}_{o} \left[\frac{(\xi J_{\rho mi}(\xi L))^2}{\xi} + \xi J^2_{\phi mi}(\xi L) \right] d\xi = 1 \tag{2.41}$$

The normalized currents can now be calculated via:

$$\hat{J}^c_{zmi}(\zeta L) = \pi J^c_{zmi}(\zeta L)/|H| \tag{2.42a}$$

$$\rho\hat{J}^c_{\rho mi}(\xi L) = \pi\rho J^c_{\rho mi}(\xi L)/|H| \tag{2.42b}$$

$$\hat{J}^c_{\phi mi}(\zeta L) = \pi J^c_{\phi mi}(\zeta L)/|H| \tag{2.42c}$$

$$\hat{J}^c_{\phi mi}(\xi L) = \pi J^c_{\phi mi}(\xi L)/|H| \tag{2.42d}$$

where

$$H_{mi}^2 = \int_0^{0.5} [J_{zmi}^2(\zeta L) + J_{\phi mi}^2(\zeta L)]d\zeta$$

$$- 2\alpha \int_{\frac{1}{2}\alpha}^{2a_o\alpha} \left[\frac{(\xi J_{\rho mi}(\xi L))^2}{\xi} + J_{\phi mi}^2(\xi L) \right] d\xi \ . \qquad (2.43)$$

To complete the SEM description, the normalization constant must be computed. Recall, from Eq.(2.38b) that the normalization constant's definition is

$$\beta_{mi} = < \bar{J}_{mi}(\bar{r}) \ ; \ \frac{\partial}{\partial s} (\bar{\bar{\Gamma}}(\bar{r},\bar{r}',s_{mi})) \ ; \ \bar{J}_{mi}(\bar{r}') > \qquad (2.44)$$

The factor involving the derivative of the impedance matrix, with respect to the complex frequency s, is the only factor in (2.44) still unspecified. This factor may be computed analytically by differentiating each of the equations in (2.24) with respect to s. Once this derivative is computed, the normalization can be found.

2.4 Validation of the Computer Code

Throughout its development, the computer code that generated the data reported herein, was tested against Glisson and Wilton's BOR code. In the testing, corresponding matrix elements were required to agree within three significant figures. The BOR code was adapted to work with complex frequencies, and again three significant figures of concurrence was required. The derivative of the impedance matrix, used in the calculation of the normalization constants, was checked against a contour integration method of Umanshankar and Wilton [17]. The normalization constants

in this report were calculated by numerically evaluating the analytically obtained derivatives. The contour method finds the derivative by numerical evaluation of Cauchy's integral formula for derivatives. The two methods of calculating the derivative again agreed to more than three significant figures.[1]

Looking ahead to Chapter 3, actual data validation is secured. A look at some of the results reported in chapter 3 is warranted. Melson [8] calculated the location on the imaginary axis of some of the cylindrical waveguide resonances. Melson found a series of open cylinder poles, that although they had distinctly non-zero real parts, were nonetheless clearly indentifiable as corresponding to his calculated waveguide resonances. In agreement with intuition, it will be observed in the present work, that as the cylinder ends are progressively closed, the cylinder pole tracks toward the purely, imaginary waveguide resonance. The closed cylinder pole was observed to approximate the corresponding waveguide resonance to a degree limited principally by the numerical error in the pole search.

---

[1] The contour method, being iterative, requires a sequence of matrix evaluations. In practice, the contour method converged with only two evaluations. The time necessary to evaluate the matrix twice is only slightly more than that needed to compute the analytic derivative. The contour method requires minimal programming, while a great effort is needed to both program and validate the analytic derivative computation.

CHAPTER 3

INTERPRETATION OF RESULTS

3.1 Introduction

In this chapter we present SEM parameters for various thicknesses of closed cylinders. Natural frequencies and representative natural modes are given in the cases of zeroth and first order azimuthal variations. Representative natural modes are discussed. Physical interpretation of the data is also undertaken. The data presented was obtained through implementation of the problem formulation presented in Chapter 2. All of the poles presented occur in the second quandrant, conjugates of these poles are themselves natural resonances of the structure. Furthermore, the singularity expansion given in (2.28) spans both positive and negative values of the modal index m. The poles associated with -m are identical to those associated with +m, since $\exp(+jm\phi)$ simply characterizes geometrically degenerate azimuthal variations.

It was observed in the construction and validation of the computer code, that the calculations were particularly sensitive to the computed value of the edge current at the so-called self zone. At this zone, current is turning the sidewall-cap edge, and electric field is being matched at the edge. This self matrix element is the largest element matrix. Errors in the calculation of this matrix element were particularly prone to induce significant errors in the pole locations. Such sensitivity of the pole location to numerical errors in other individual matrix elements is not observed.

Using a technique that determines pole multiplicity suggested by Marin [7], sample poles were shown to be simple (multiplicity one). It is well known that the poles must have finite order; but their simpleness was assumed on the basis of heuristic arguments. It is known that topologically similar structures such as the sphere and prolate spheroid have simple poles. If a pole is simple, the determinant of the impedance matrix is zero, and the determinant of the impedance matrix derivative is nonzero. The impedance matrix derivative is calculated in the normalization constant computation, so the pole multiplicity was checked as an adjunct to the normalization constant determination.

3.2 Zeroth Order Azimuthal Variation

Figure 3 shows natural resonance trajectories as the aspect ratio varies for two structures in the case of zeroth-order azimuthal variation. Recall, from Chapter 2, that aspect ratio is the length-to-diameter ratio. Figure 3a shows the pole trajectories for the capped cylinder as the aspect ratio progresses through the values: 100, 50, 20, 10, 5, and 3.3333, while Figure 3b shows comparable data for the open cylinder. The data given are the resonances lying nearest the $j\omega$ axis for the individual aspect ratios. Additional resonances for the structures lie deeper into the left-half plane, these poles represent more strongly damped resonances. Being more strongly damped, these resonances are of much less practical significance in the SEM expansion than their less damped counterparts.

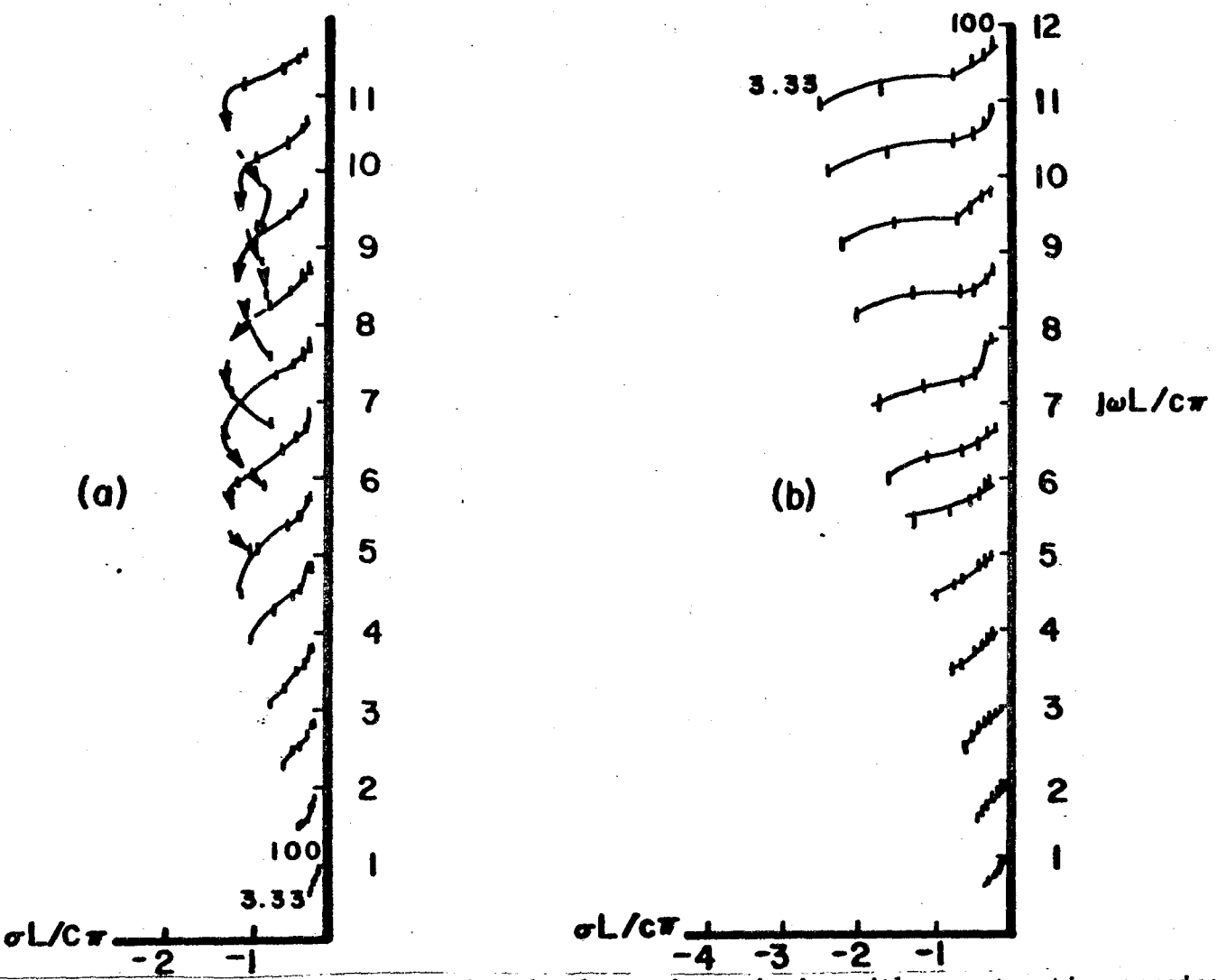

Figure 3. Pole trajectories for zeroth-order harmonic variation with aspect ratios ranging from 100 to 3.3333: (a) closed cylinder, (b) open cylinder. Ticks on the trajectories indicate aspect ratio evaluations at: 100, 50, 20, 10, 5, 3.3333.

As Melson observed with the open cylinder and Tesche with the thin wire, the zeroth-order poles tend to move downward and outward as the cylinder thickens. This phenomenon corresponds to a decrease in resonant frequency and an increase in the damping factor as the cylinder becomes thicker. Said differently, the quality factor (Q) for the $m = 0$ modes decreases with decreasing aspect ratio (thicker cylinders). The Q is defined [18] as

$$Q = \frac{|s|}{2\sigma} \tag{3.1}$$

where $s = -\sigma + j\omega$ is the complex resonance. Further similarities between the two data sets are immediately evident. For the first few resonances of each aspect ratio, the closed cylinder pole trajectories very nearly track the corresponding open-cylinder pole trajectories. This nearness of the open and closed cylinder resonances also persists among all the thin (large aspect ratio) cylinders' natural frequencies. The departures between trajectories for the two structures—i.e. the differences in the Q's for the structures—appear only for the higher frequency resonances of relatively thick structures. The distinguishing feature between the geometries in this circumstance is a significant electrical size of the caps on the closed structure.

For a radiating structure, a lower Q indicates a greater propensity for the given resonant mode to radiate. We may draw from this fact some heuristic inferences about the radiation mechanisms that produce changes in Q. The principle mechanism is the acceleration of charge, as current flows between the cylinder and caps—i.e. z-directed current on the wall and ρ-directed current

on the caps exchange charge between the respective surfaces. Consequently, a large current magnitude at the cylinder cap junctions implies a strong propensity to radiate. For the seventh resonance (nominally) and higher, the Q of the structure does not vary monotonically with aspect ratio. We observe from Figure 3a that the pole trajectories begin to bend back toward the $j\omega$ axis as the aspect ratio decreases, and that for the eleventh and twelth resonances, the trajectory inflects a second time, and migrates outward again. This behavior is markedly like the behavior of the resonances of the L-wire, studied by Umashankar and Wilton, [19]. In their study, pole trajectories were plotted as a function of the ratio of lengths of the arms of the L-wire with the poles normalized to the length of the longer arm. This representation is analogous to the one for the capped-cylinder used here (after all, an L-shaped generatrix describes the capped cylinder).

The L-wire data indicate an inward inflection of pole trajectories as the length of the shorter arm approaches that of a resonant wire. Essentially the same phenomenon is manifested by the capped cylinder through the present data. Figure 4 shows the longitudinal natural mode current profile for, respectively, the sixth (4a) and ninth (4b) resonances of the capped cylinder, whose aspect ratio is 3.3333. The sixth pole for this structure is the final one on the sixth trajectory in Figure 3a—a trajectory along which Q decreases monotonically—while the ninth resonance lies at the end of a trajectory on which the Q first minimizes and then begins to increase. We observe that the caps are nearly resonant for the latter case (Figure 4b) since their radial currents appear to attain

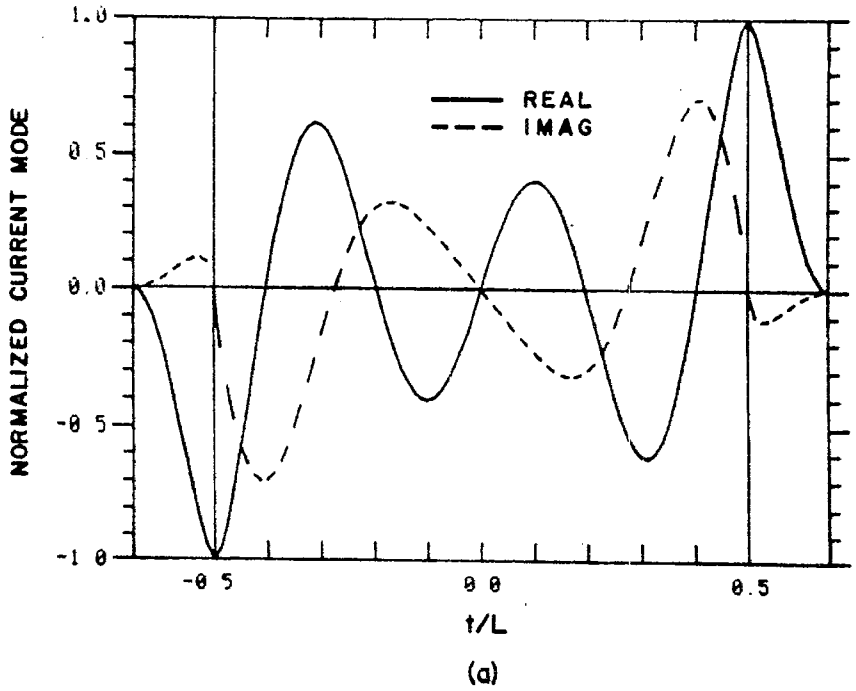

(a)

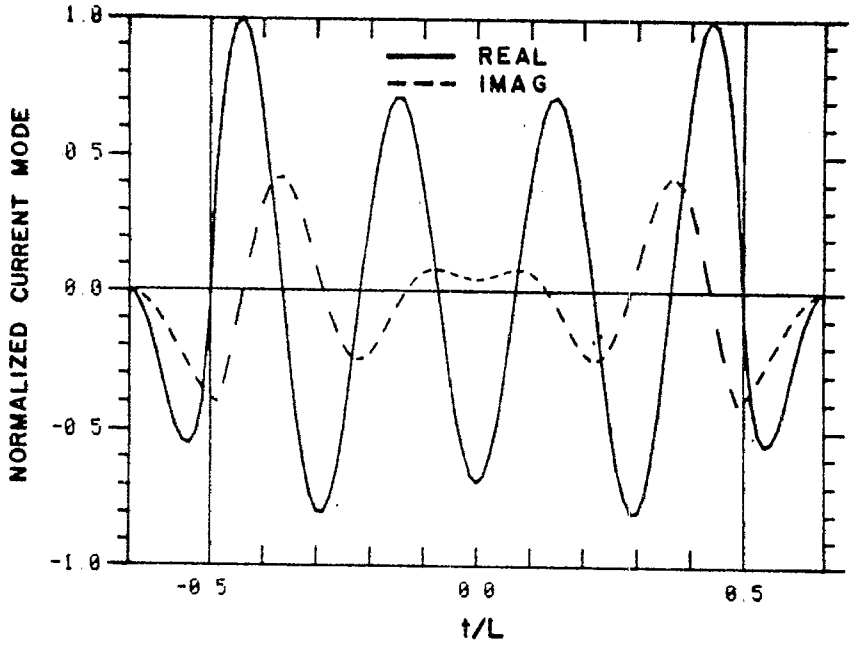

(b)

Figure 4. Current natural modes for the zeroth harmonic mode, aspect ratio 3.3333: (a) sixth current natural mode, (b) ninth natural mode. The central region between the vertical bars on each graph shows current flowing on the cylinder sidewalls, while the extreme regions between the vertical lines and the ends of the graph show the current that flows on the caps.

a local minimum at the rims. In contrast, the current mode for the sixth resonance manifests large current densities flowing around the rims. Thus the greater propensity to radiate associated with the ninth mode, and its Q is concomitantly lower. The inward inflection of the ninth pole trajectory can be explained as a decreasing propensity to radiate as the caps and the cylinder wall resonate more-or-less independently and the current across the rim is small.

The data given in Figure 3a are poles arising from zeros of the B_{11} operator in (2.7). The closed cylinder has a second set of zeroth-order modes, since in the $m=0$ case, the J_t and J_ϕ components of current decouple. The operators B_{11} and B_{22} of (2.7) have respective sets of singularities, that are independent of one another. The poles due to zeros of B_{11} are the ones reported herein. They correspond to resonances in longitudinal current. The resonances associated with zeros of B_{22} are counterpart to the $m=0$ resonances of a loop structure as, for example, Umashankar presents in [20]. These loop resonances cannot be excited by a time harmonic excitation because of their azithumal invariance, therefore, they are not addressed further.

3.3 Comparison with Prolate Spheroid Mode Zero Poles

It is interesting to compare the resonances of the capped cylinder with a closely related structure often used to model cylinders, namely, the prolate spheroid. We consider spheroids which inscribe the cylinder. Figure 5 shows pole trajectories for the closed cylinder, prolate spheroid, and open cylinder. The prolate spheroid pole trajectories are graphed from natural resonances calculated by Marin [7]. The aspect ratios for which

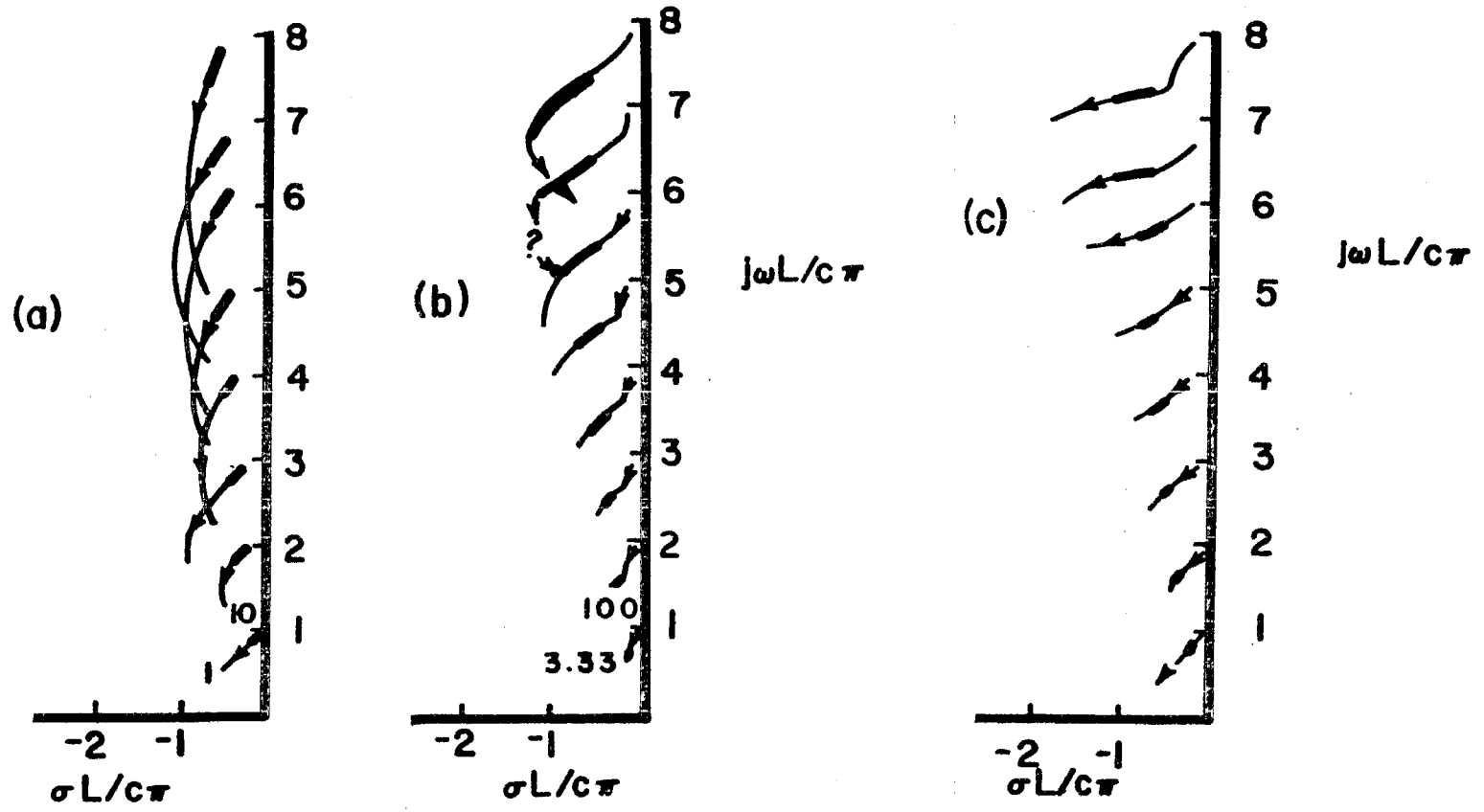

Figure 5. Pole trajectories for zeroth harmonic mode variation: (a) prolate spheroid, (b) closed cylinder, (c) open cylinder. Aspect ratios common to the three sets of trajectories are highlighted.

Marin determined poles were 10, 5, 2, and 1. The common range of aspect ratio (10 — 5) is highlighted in each graph of Figure 5. As stated in Chapter 1, the prolate spheroid has been used for nearly a century to model cylindrical antennas and scatterers. Poles for the three structures shown in Figure 5, have interesting similarities. Whereas the pole trajectories for both the prolate spheroid and the closed cylinder exhibit some migration away from and then toward the imaginary axis with decreasing aspect ratio; the open cylinder does not display this behavior. This alternate migration, however, occurs in a less pronounced fashion for the the prolate spheroid than it does for the closed cylinder, and its onset is higher in frequency. For the poles shown, the prolate spheroid poles move inward only for the extreme aspect ratios of 2 and 1.

The difference in degree of the poles trajectory migration between the closed cylinder and the prolate spheroid and absence of such a phenomenon in the open cylinder is explained by the extent to which charges on each structure accelerate. The power flux density radiated from a scatterer is proportional to a factor of charge acceleration on the structure. Charges on the open cylinder accelerate principally as they approach the cylinder ends, where the currents vanish; charges on the prolate spheroid accelerate steadily over the whole structure as the current conforms to the spheroid's curvature; charges on the closed cylinder, by comparison, accelerate abruptly as they approach the cap-sidewall edge and somewhat less so at the cap centers.

In reference to Figure 6, the natural mode for the dominant resonance of aspect ratio 3.3333, it is seen that the current density has a slope discontinuity near the cap-sidewall edge. This slope discontinuity is proportional to a factor of charge acceleration in the power flux density. Computations of the quality factor of each structure, reveal that at the dominant resonance, the three structures have nearly equal Q's; at all other resonances, however, the prolate spheroid has a Q as much as fifty percent higher than that of the open cylinder. The open cylinder, meanwhile has a quality factor ten percent in excess of the closed cylinder's. Though the prolate spheroid continuously sheds energy because of torsional radiation, it is still a better resonator than either cylinder.

Other comparisons between the pole distributions of the three structures are possible. Page and Adams [3] contend that the prolate spheroid more accurately models the capped cylinder if the spheroid is somewhat thicker and longer than the corresponding capped cylinder. Although the first few pole trajectories of each structure lie close to one another, it does not appear that thickening and lengthening the prolate spheroid will induce better agreement with the poles of the closed cylinder for these trajectories. Apparently, Page and Adams' statement must be qualified to apply to the first resonance of the structures only.

3.4 First Order Azimuthal Variation

Figure 7a shows pole trajectories for the first four poles of each aspect ratio (100, 50, 20, 10, 5, 3.3333) in the case of first order azimuthal variation. Figure 7b shows comparable data for an

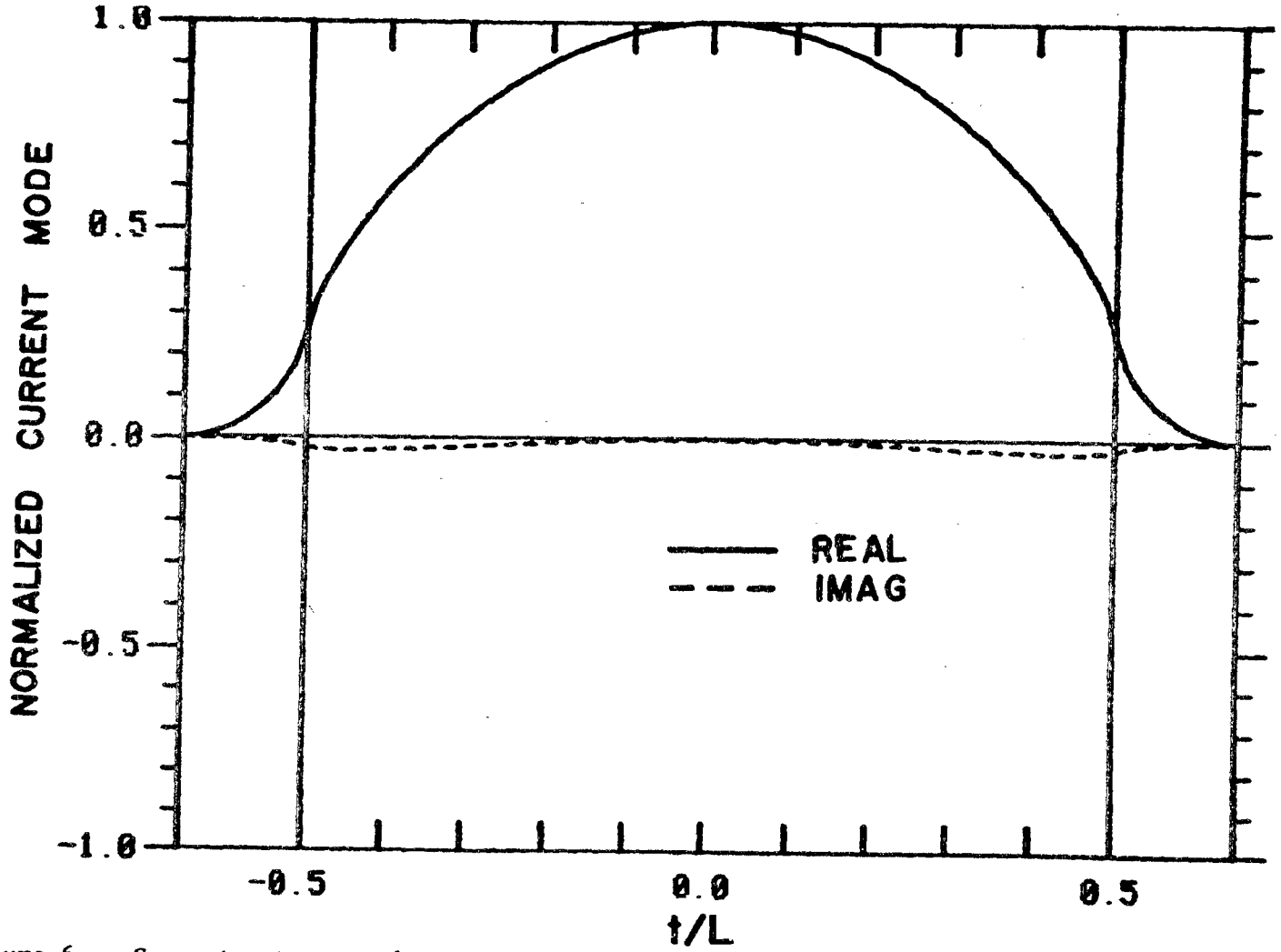

Figure 6. Current natural mode for the dominant resonance of aspect ratio 3.3333 for the zeroth harmonic mode. The current of the cylinder sidewall is shown in the central region between the vertical lines; the cap currents are shown to the left and to the right of this region.

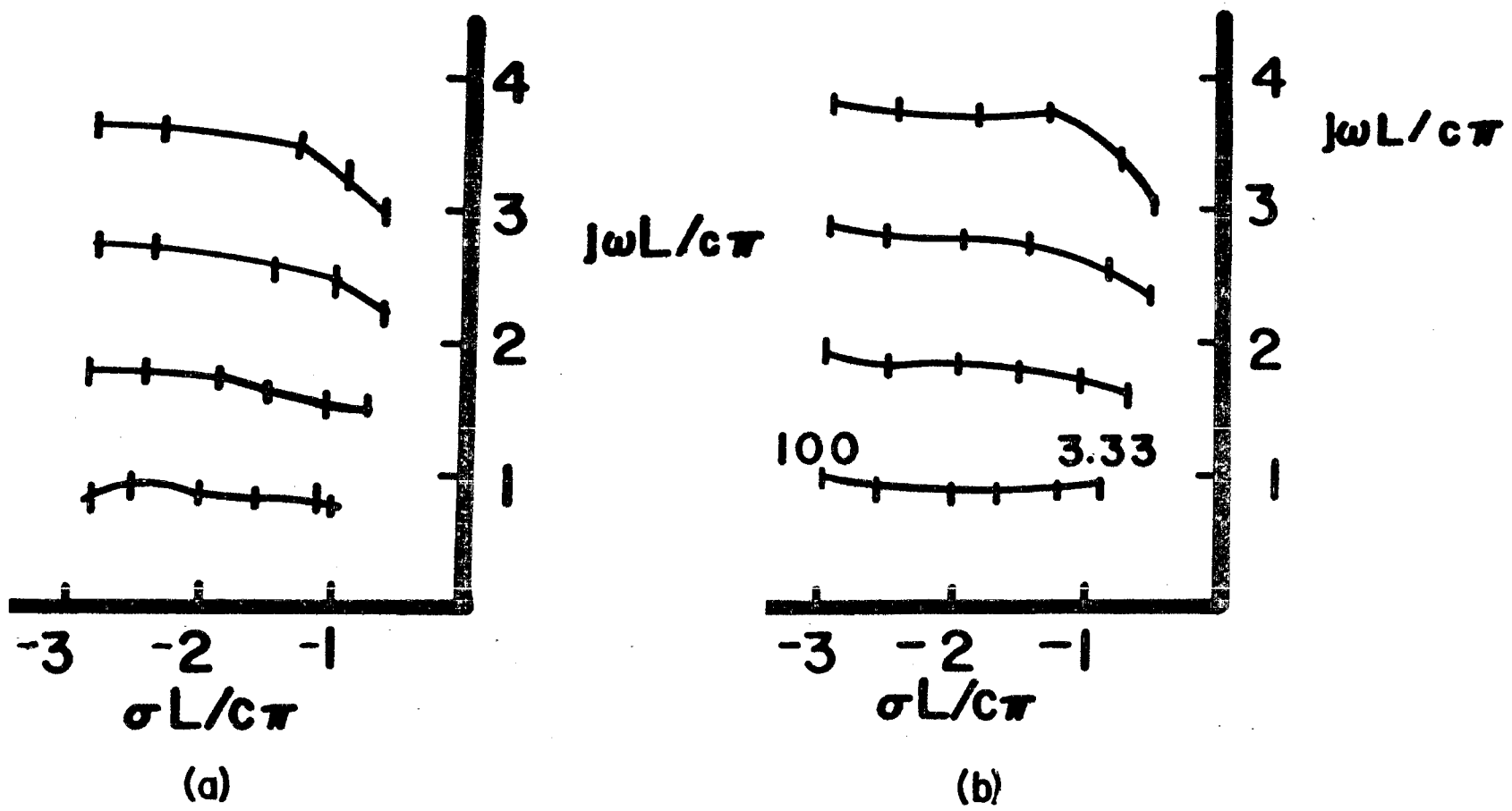

Figure 7. Pole trajectories for cylinder aspect ratios between 100 and 3.3333 for the first harmonic mode: (a) closed cylinder, (b) open cylinder. Ticks on the trajectories indicate aspect ratio evaluations at 100, 50, 20, 10, 5, 3.3333.

open cylinder. Corresponding poles in the open and closed cases occur in close proximity to one another, hence, the pole trajectories in the open and closed cases are nearly parallel. Both sets of poles are decreasingly damped as the aspect ratio decreases. This trend is opposite to that of the zeroth order poles. Since this phenomenon has been observed by Melson in the geometrically simpler open cylinder, this reversal of pole trajectory progression is accomplished only by the presence of azimuthally varying current densities. These azimuthally varying currents contribute to the torsional radiation via charge acceleration due to variation in the azimuthal direction. This torsional radiation effect is strong enough so that the Q increases as aspect ratio decreases. For the sample data presented, effects of the endcaps are not as pronounced as in the mode zero case, and the torsional radiation mechanism appears to dominate over endcap effects. The closed cylinder, however, is a lower Q structure than the open cylinder.

3.5 Interior Resonances

The basis of this work's formulation, the electric field integral Equation 2.2, does not discriminate between interior and exterior excitations. In each case of azimuthal variation, a collection of interior resonances occur. These interior resonances occur in layers emerging for increasingly thinner cylinders as the frequency increases. These natural resonances are analogous to poles of the circular loop that belong to the so-called Type III portion of eigensets [21] (the exterior resonances discussed in previous sections are members of the Type II portion of eigensets).

These interior resonances are characterized as being purely imaginary. The location of these interior resonances (as opposed to the exterior resonances) can be determined analytically using waveguide theory. The pole locations are obtained by modeling the cylinder as a cylindrical cavity of length L, capped by perfect magnetic or electric conducting sheets. A collection of these interior resonances is calculated and presented by Melson [8]; some of these calculated pole locations are listed in the table.

MODE	CAVITY POLE	CLOSED CYLINDER POLE	OPEN CYLINDER POLE
TM_{011}	j5.20	-.000034 + j5.20	-.031 + j5.42
TM_{012}	j5.48	.00026 + j5.48	-.084 + j5.78
TM_{111}	j8.19	.019 + j8.22	-.018 + j8.34
TE_{111}	j4.03	-.00023 + j4.02	-.056 + j4.02
TE_{112}	j4.39	-.0025 + j4.33	-.22 + j4.30
TE_{211}	j6.56	.00034 + j6.55	-.025 + j6.55

The table presents a few selected interior resonances in the open cylinder case, the closed cylinder case, and the corresponding exact cavity pole. Because the tube has open ends, it radiates energy, consequently, the open cylinder interior resonances have appreciable real parts and hence are not purely oscillatory. Wilton has conjectured that the open cylinder poles would migrate to the corresponding waveguide resonance if the cylinder were capped by perfectly conducting material. Indeed, the closed cylinder, since it confines interior excitations within an electric

perfectly conducting shell, has poles with much smaller real parts, that arise principally from numerical inaccuracies in the pole search procedure. Near the imaginary axis, the poles are weakly defined by (2.31) and both contour searching and Muller's method encounter difficulty in searching for a pole there. To observe the open and closed cylinder Type III poles coalesce, a hole was opened in both endcaps. The hole radius ranged through 1/4, 1/2, and 3/4 of the cylinder outer radius. Figure 8 shows the poles tracking a smooth path from the open cylinder case to the closed cylinder case.

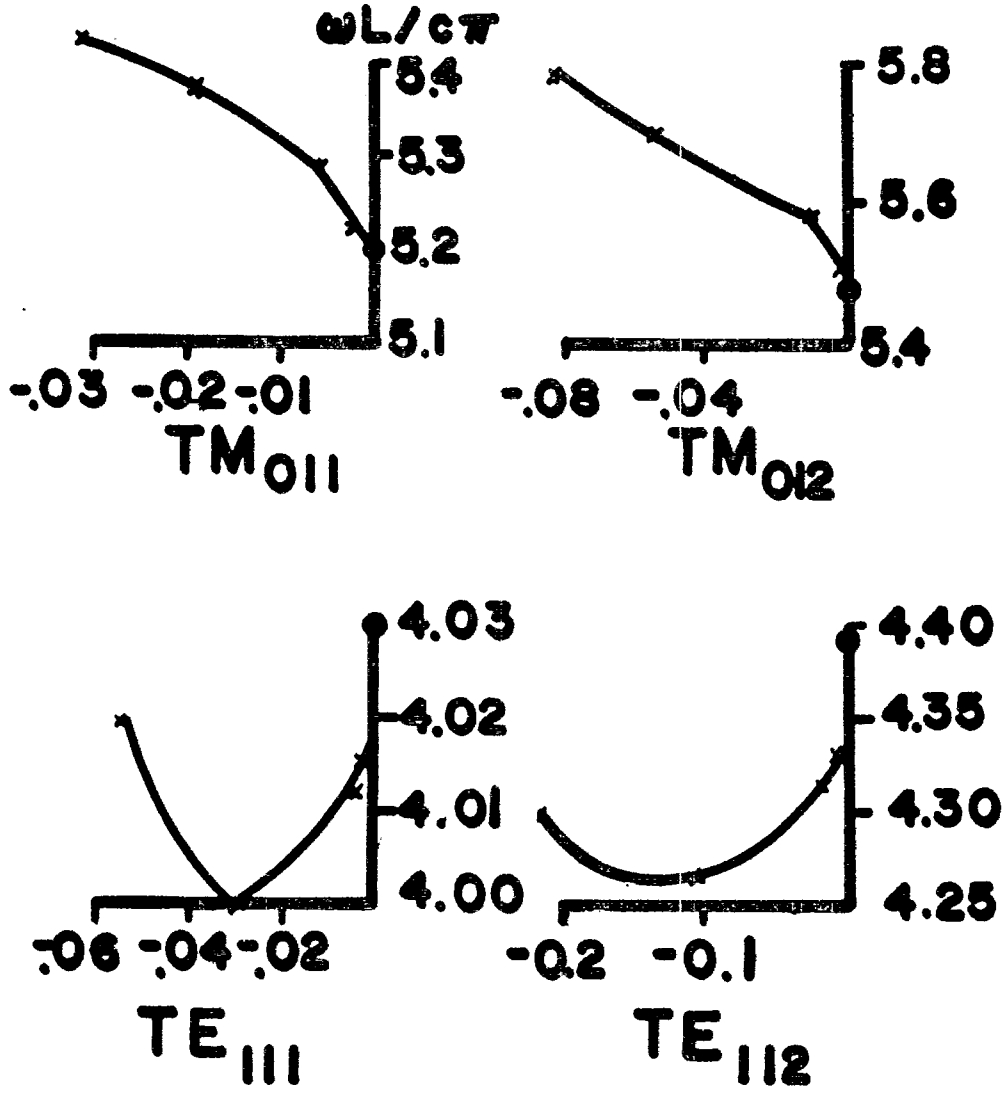

Figure 8. Pole trajectories of selected interior resonances showing the migration of the poles as the cylinder endcaps are closed. A solid dot designates the location of the purely imaginary cavity resonance for each mode. The pole locations correspond to the poles of a cylinder with aspect ratio 3.3333, these locations are marked with an x. The ratio of inner to outer radius of the endcaps ranges through the values 1.0, 0.75, 0.50, 0.25, and 0.00, moving from left to right on the graph.

CHAPTER 4

CONCLUSIONS

A representative group of Singularity Expansion Method parameters for a closed perfectly cylinder are presented herein. The complete tabulation of the data obtained in this work is presented in a companion report [12].

One significant contribution of this work is the collection of the parameters themselves, particularly the natural resonances. The capped cylinder, although a structure of much practical significance, had not had its natural frequencies computed and catalogued. Attempts to determine such data inevitably depended upon significant geometrical simplifications, such as use of prolate spheroids or tubes, as approximating structures. Availability of non-zeroth order natural frequencies allows additional accuracy of the SEM expansion as well as affording greater insight into the scattering properties of the capped cylinder. Poles lying nearer the vertical axis contribute more strongly to the SEM description; since mode one pole trajectories are contradirected from those of mode zero, conceivably mode one poles could contribute significantly to the SEM description. Competition for dominance in the SEM description could extend to even higher order modes. It is expected, however, that the coupling coefficients will diminish appreciably for nonzeroth order natural modes, thus weakening higher harmonic order pole influences. Melson reminds that this issue should be remembered whenever coupling coefficients are calculated. Although coupling coefficient

computation is beyond the scope of this work, it will be an inevitable and enlightening exercise in this data's application.

The discussion in Chapter 3 on the torsional effects experienced by charges on the capped cylinder are intrinsically qualitative and preliminary. Further investigation of this phenomenon will likely augment and supplant the physical interpretation of the data presented here. Although accurately plotting current streamlines associated with the present data would be helpful, as Melson suggests for the open cylinder, and as Howard [21] has done for the sphere, it is anticipated that such work for the capped cylinder will be more difficult than for these other structures. This difficulty is foreseen for the same reason that the cylinder has elluded analytical solution, namely, that the capped cylinder does not conform to a separable geometry. Through numerical techniques in the geometrical theory of diffraction these difficulties may be resolved.

Since the capped cylinder formulation used here allows the possibility of holes in the cylinder endcaps, modeling of coaxial structures should be possible. Further work would naturally include equivalent circuit synthesis for such a coaxial structure. It would also be interesting to calculate additional mode one poles, in an effort to detect effects on pole distribution directly attributable to the presence of endcaps on the tube. Investigation and analysis of higher harmonic natural modes would also be interesting, since little is known about these modes.

REFERENCES

[1] Abraham, M., "Die Electrischen Schwingungen um einen stabformigen Leiter, behandelt nach der Maxwell'schen Theorie," Ann. D. Physik, Vol. 66, pp. 435-472, October, 1898.

[2] Page, L., and N. T. Adams, "The Electrical Oscillations of a Prolate Spheroid Paper I," Phys. Rev., Vol., 53, pp. 819-831, 1938.

[3] Page, L., "The Electrical Oscillations of a Prolate Spheroid Paper II," Phys. Rev., Vol. 65, pp. 98-110, 1944.

[4] Page, L., "The Electrical Oscillations of a Prolate Spheroid Paper III," Phys. Rev., Vol. 65, pp. 111-116, 1944.

[5] Baum, C. E., "The Singularity Expansion Method," in L. B. Felsen, Ed., Transient Electromagnetic Fields, Springer-Verlag, Berlin-Heidelberg-New York, 1976.

[6] Tesche, F. M., "The Far-Field Response of a Step-Excited Linear Antenna Using SEM," IEEE Trans. Antennas Propagat., Vol. AP-23, pp. 834-838, November, 1975; also Sensor and Simulation Note 177, The Dikewood Corporation, Albuquerque, New Mexico, May, 1973.

[7] Marin, L., "Natural Mode Representation of Transient Scattering From Rotationally Symmetric, Perfectly Conducting Bodies and Numerical Results for a Prolate Spheroid," Interaction Note 119, Air Force Weapons Laboratory, Albuquerque, New Mexico, September, 1972.

[8] Melson, G. B. and L. W. Pearson, "SEM Characterization of the Electromagnetic Scattering from Thin and Thick Open-Ended Cylinders," University of Kentucky Electromagnetics Research Report, November, 1980.

[9] Mautz, J. R. and R. F. Harrington, "Radiation and Scattering from Bodies of Revolution," Appl. Sci. Res., Vol. 20, pp. 405-435, June, 1969.

[10] Glisson, A. W. and D. R. Wilton, "Simple and Efficient Numerical Techniques for Treating Bodies of Revolution," Technical Report for RADC Contract No. F30602-78-C-0120, University of Mississippi, University, Mississippi, March, 1979.

[11] Harrington, R. F., Field Computations by Moment Methods, The MacMillan Company, New York, 1968.

[12] Roberts, J. L. and L. W. Pearson, "SEM Characterization of a Closed Cylinder," Interaction Note 430, University of Mississippi, University, Mississippi, June 1982

[13] Wilton, D. R., A. W. Glisson and C. M. Butler, "Numerical Solutions for Scattering by Rectangular Bent Plane Structures," Final Report, Contract No. N00123-75-C-1372 for Naval Electronics Laboratory Center (now Naval Ocean System Center), University of Mississippi, University, Mississippi, October, 1976.

[14] Baum, C. E., "Interaction of Electromagnetic Fields with an Object which has an Electromagnetic Symmetry Plane," Interaction Note 63, Air Force Weapons Laboratory, March, 1971.

[15] Isaacson, E., and H. B. Keller, Analysis of Numerical Methods, John Wiley and Sons, New York, 1966.

[16] Singaraju, B. K., D. V. Giri and C. E. Baum, "Further Developments in the Application of Contour Integration to the Evaluation of the Zeros of Analytic Functions and Relevant Computer Programs," Mathematics Note 42, Air Force Weapons Laboratory, Albuquerque, New Mexico, March, 1976.

[17] Umashankar, K. R., and D. R. Wilton, "Parametric Study of an L-Shaped Wire Using the Singularity Expansion Method," Interaction Note 152, University of Mississippi, University, Mississippi, November, 1973.

[18] Michalski, K. A., and L. W. Pearson, "Synthesis of SEM Derived Equivalent Circuits for Electromagnetic Energy Collecting Structures," Final Report, Subtask 03-06 of Contract F29601-78-C-0082 for Mission Research Corporation, University of Mississippi, University, Mississippi, October, 1981.

[19] Umashankar, K. R. and D. R. Wilton, "Transient Scattering of an L-Shaped Wire Using the Singularity Expansion Method," IEEE Trans. Antennas Propagat., Vol. AP-23, pp. 838-841, November, 1975.

[20] Umashankar, K. R. and D. R. Wilton, "Transient Characterization of the Circular Loop Using the Singularity Expansion Method," Interaction Note 259, University of Mississippi, University, Mississippi, August, 1974.

[21] Howard, A. W., "A Geometric Theory of Natural Oscillation Frequencies in Exterior Scattering Problems," Interaction Note 378, Department of Electrical Engineering, University of Arizona, October, 1979.

BIBLIOGRAPHY

Abraham, M., "Die Electrischen Schwingungen um einen stabformigen Leiter, behandelt nach der Maxwell'schen Theorie," Ann. D. Physik, Vol. 66, pp. 435-472, October, 1898.

Baum, C. E., "Interaction of Electromagnetic Fields with an Object which has an Electromagnetic Symmetry Plane," Interaction Note 63, Air Force Weapons Laboratory, March 1971.

Baum, C. E., "The Singularity Expansion Method," in L. B. Felsen, ed., Transient Electromagnetic Fields, Springer-Verlag, Berlin-Heidelberg-New York, 1976.

Glisson, A. W. and D. R. Wilton, "Simple and Efficient Numerical Techniques for Treating Bodies of Revolution," Technical Report for RADC Contract No. F30602-78-C-0120, University of Mississippi, University, Mississippi, March, 1979.

Harrington, R. F., Field Computations by Moment Methods, The MacMillan Company, New York, 1968.

Howard, A. Q., "A Geometric Theory of Natural Oscillation Frequencies in Exterior Scattering Problems," Interaction Note 378, Department of Electrical Engineering, University of Arizona, October, 1979.

Isaacson, E., and H. B. Keller, Analysis of Numerical Methods, John Wiley and Sons, New York, 1966.

Marin, L., "Natural Mode Representation of Transient Scattering From Rotationally Symmetric, Perfectly Conducting Bodies, and Numerical Results for a Prolate Spheroid," Interaction Note 119, Air Force Weapons Laboratory, Albuquerque, New Mexico, September, 1972.

Mautz, J. R. and R. F. Harrington, "Radiation and Scattering from Bodies of Revolution," Appl. Sci. Res., Vol. 20, pp. 405-435, June, 1969.

Melson, G. B. and L. W. Pearson, "SEM Characterization of the Electromagnetic Scattering From Thin and Thick Open-Ended Cylinders," University of Kentucky Electromagnetics Research Report, November, 1980.

Michalski, K. A., and L. W. Pearson, "Synthesis of SEM Derived Equivalent Circuits for Electromagnetic Energy Collecting Structures," Final Report, Subtask 03-06 of Contract F29601-78-C-0082 for Mission Research Corporation, University of Mississippi, University, Mississippi, October, 1981.

Page, L., and N. T. Adams, "The Electrical Oscillations of a Prolate Spheroid Paper I," Phys. Rev., Vol. 53, pp. 819-831, 1938.

Page, L., "The Electrical Oscillations of a Prolate Spheroid Paper II," Phys. Rev., Vol. 65, pp. 98-110, 1944.

Page, L., "The Electrical Oscillations of a Prolate Spheroid Paper III," Phys. Rev., Vol. 65, pp. 111-116, 1944.

Roberts, J. L. and L. W. Pearson, "SEM Characterization of a Closed Cylinder," University of Mississippi, University, Mississippi, June, 1982.

Singaraju, B. K., D. V. Giri and C. E. Baum, "Further Developments in the Application of Contour Integration to the Evaluation of the Zeros of Analytic Functions and Relevant Computer Programs," Mathematics Note 42, Air Force Weapons Laboratory, Albuquerque, New Mexico, March, 1976.

Tesche, F. M., "The Far-Field Response of a Step-Excited Linear Antenna Using SEM," IEEE Trans. Antennas Propagat., Vol. AP-23, pp. 834-838, November, 1975; also Sensor and Simulation Note 177, The Dikewood Corporation, Albuquerque, New Mexico, May, 1973.

Umashankar, K. R. and D. R. Wilton, "Parametric Study of an L-Shaped Wire Using the Singularity Expansion Method," Interaction Note 152, University of Mississippi, University, Mississippi, November, 1973.

Umashankar, K. R. and D. R. Wilton, Transient Characterization of the Circular Loop Using the Singularity Expansion Method," Interaction Note 259, University of Mississippi, University, Mississippi, August, 1974.

Umashankar, K. R. and D. R. Wilton, "Transient Scattering of an L-Shaped Wire Using the Singularity Expansion Method," IEEE Trans. Antennas Propagat., Vol. AP-23, pp. 838-841, November, 1975.

Wilton, D. R., A. W. Glisson and C. M. Butler, "Numerical Solutions for Scattering by Rectangular Bent Plane Structures," Final Report, Contract No. N00123-75-C-1372 for Naval Electronics Laboratory Center (now Naval Ocean System Center), University of Mississippi, University, Mississippi, October, 1976.